Geosci. Model Dev. Discuss., 8, 4487–4544, 2015
www.geosci-model-dev-discuss.net/8/4487/2015/
doi:10.5194/gmdd-8-4487-2015

Geoscientific Model Development Discussions
Open Access

SiSeRHMap v1.0: a simulator for mapped seismic response using a hybrid model

G. Grelle[1], L. Bonito[2], A. Lampasi[3], P. Revellino[2], L. Guerriero[2], G. Sappa[1], and F. M. Guadagno[2]

[1]Department of Civil and Environmental Engineering, University of Rome “La Sapienza” via Eudossiana, 18 – 00184 Rome, Italy
[2]Department of Science and Technologies, University of Sannio, via Dei Mulini 59/A – 82100 Benevento, Italy
[3]ENEA Frascati Research Center, Via Enrico Fermi 45, 00044 Frascati (Rome), Italy

Received: 19 March 2015 – Accepted: 21 May 2015 – Published: 17 June 2015

Correspondence to: G. Grelle (gerardo.grelle@unisannio.it)

Published by Copernicus Publications on behalf of the European Geosciences Union.

Abstract

SiSeRHMap is a computerized methodology capable of drawing up prediction maps of seismic response. It was realized on the basis of a hybrid model which combines different approaches and models in a new and non-conventional way. These approaches and models are organized in a code-architecture composed of five interdependent modules. A GIS (Geographic Information System) Cubic Model (GCM), which is a layered computational structure based on the concept of lithodynamic units and zones, aims at reproducing a parameterized layered subsoil model. A metamodeling process confers a hybrid nature to the methodology. In this process, the one-dimensional linear equivalent analysis produces acceleration response spectra of shear wave velocity-thickness profiles, defined as trainers, which are randomly selected in each zone. Subsequently, a numerical adaptive simulation model (Spectra) is optimized on the above trainer acceleration response spectra by means of a dedicated Evolutionary Algorithm (EA) and the Levenberg–Marquardt Algorithm (LMA) as the final optimizer. In the final step, the GCM Maps Executor module produces a serial map-set of a stratigraphic seismic response at different periods, grid-solving the calibrated Spectra model. In addition, the spectra topographic amplification is also computed by means of a numerical prediction model. This latter is built to match the results of the numerical simulations related to isolate reliefs using GIS topographic attributes. In this way, different sets of seismic response maps are developed, on which, also maps of seismic design response spectra are defined by means of an enveloping technique.

1 Introduction

In the scientific community, it is well known that lithologic stratigraphy as well as topographic features are capable of considerably amplifying the local destructive action of an earthquake (Del Prete et al., 1998; Athanasopoulos et al., 1999). Thus, in prone areas, seismic microzonation studies assume an important role in urban planning and

GMDD
8, 4487–4544, 2015

seismic risk management (Lachet et al.,1996; Bianchi Fasani et al., 2008; Compagnoni et al., 2011; Milana et al., 2011; Grasso and Maugeri, 2012; Moscatelli et al., 2013). As a consequence, methods for high levels of seismic microzonation (mapped seismic response studies) aim at providing quantitative data for use in building design (Borcherdt, 1994; Todd and Harris, 1995; Dan, 2005; Kokošin and Gosar, 2013). Many building codes, such as Euro Code 8 and FEMA 356 (2000), require seismic design actions defined by simplified elastic acceleration spectra deriving from local grassroots hazard and site amplification effects.

In addition to a need to have a sufficient amount of information suitable for seismic microzonation, computerized data management and spatial distribution in terms of input and output/outcomes, is also a requirement. Therefore, the Geographic Information Systems (GIS) contribute the most to maximizing the available data, in the assessment or estimation of ground-motion amplification (Kolat et al., 2006; Ganapathy, 2011; Hashemi and Alesheikh, 2012; Turk et al., 2012; Hassanzadeh et al., 2013) and seismic-induced effects (Grelle et al., 2011; Grelle and Guadagno, 2013).

In this aforementioned context, SiSeRHMap provides synthetic multi-map data regarding a complex phenomenon, such as seismic site response, on the basis of a new hybrid methodology in which a metamodeling process is the core feature. In recent years, the use of the metamodels in many engineering and environmental science fields (Lampasi et al., 2006; Yazdi and Neyshabouri, 2014; Wang et al., 2014; Hong et al., 2014), together with GIS supported analysis (Reed et al., 2012; Fan et al., 2015; Soares et al., 2014), has produced good performances, providing fast versatility and rapid updating. Thus, in areas with a not very high geological complexity, the proposed methodology can present a high computational efficiency in comparison to expensive rigorous physically based models. This aspect is reflected in a balanced compromise between the accuracy and robustness required and computational easiness and magnitude of the analyzed area. The mapped seismic response provided by SiSeRHMap has a uniform and equivalent areal coverage, due to the fact that the method does not carry out the interpolation of single-point data-outputs, as usually occurs in GIS-

GMDD
8, 4487–4544, 2015

supported methodologies. In contrast to 2-D and 3-D physically based codes in which the full spectral seismic response is provided only for a limited number of assigned points, SiSeRHMap provides a complete spectral response in any surface point. In addition, the geo-referenced data, provided by the presented computerized methodology, can assume a very important role in seismic risk management, as well as in seismic building design strategy.

1.1 Code design and aims

SiSeRHMap is a computer program methodology aimed at the mapped Simulation of the site Seismic Response using a Hybrid Model. The Hybrid Model consists of a complex computational system composed of a GIS frame model, analytical models (physically-based) and metamodeling procedures. SiSeRHMap is capable of developing map-sets of seismic response taking into account the combined effects of plane-parallel stratigraphy and real topographic features.

SiSeRHMap is composed of five progressive inter-depending Python compute modules, each of which necessitates an external input data. The input data and dataset are inserted or linked into a Textual User Interface (TUI) which writes the file "Instruction.txt" that the Python modules read in running.

The modules and their computational functions are as follows:

- mod.1: Lithodynamic Units parameterization;
- mod.2: Gis Cubic Model frame;
- mod.3: Stratigraphic Response;
- mod.4: Training "Spectra";
- mod.5: GCM Maps Executor.

GMDD
8, 4487–4544, 2015

1.2 Background

In mapped seismic response studies carried out using analytical methods for assessing or estimating stratigraphic seismic site responses, the GIS provides the spatial distribution of parameters which characterize the seismic motion (Jimenez et al., 2000; Sokolov and Chernov, 2001; Nath, 2004; Kienzle et al., 2006). Based on a multivariate regression analysis of common recurrent regional data-settings regarding simple sequences, procedures for calculating seismic soil response have also been introduced (Rodriguez-Marek et al., 2001; Papadimitriou et al., 2008).

Among the above-mentioned GIS based models, Grelle et al. (2014) have recently introduced a hybrid model, based on the "GIS Cubic Model (GCM)" frame which is, in turn, based on the concept of lithodynamic units and zones. Here, a lithodynamic unit is defined as a lithological unit which is characterized by a shear wave velocity depth-dependent curve and subsequently by non-linear stress–strain behaviour. The zone is defined by a specific combination, in sequence, of lithodynamic units. The hybrid model computes the mapping of seismic response using an adaptive model which is trained on 1-D seismic response target-cases calculated from some shear wave velocity-thickness sequences; these latter are uniformly randomly selected in coherence with general lithodynamic layered models assumed for the study area. In this way, the trained adaptive model, conceptually defined as a metamodel (replacement model), is used in the spatial predictive analysis which aims at developing seismic response maps by means of its metamodel solving in the GCM.

Topographic amplification is a more relevant frequency dependent effect in zones characterized by hill and mountain features (Çelebi, 1987; Kawase and Aki, 1990; Assimaki et al., 2005; Del Gaudio and Wasowski, 2007; Hough et al., 2010; Massa et al., 2010; Pischiutta et al., 2010). 2-D and 3-D simulation analytical approaches on different relief shapes, as well as different incident seismic wave motions, have been introduced (Sánchez-Sesma, 1983; Geli et al., 1988; Ashford et al., 1997; Durand et al., 1999; Maufroy et al., 2012, 2015). Geli et al. (1988) used numerical methods for assessing the topographic amplification factor, A_T, of the vertical incident of horizontal shear wave (SH) on 2-D isolated reliefs constituted by uniform material and different layering structures. Their results highlighted that the frequency-depending amplification factors change considerably along the topographic surface, showing a greater amplification at the ridge, reaching values over 2.00 in some cases. Ashford et al. (1997) quantified the theoretical effect of the horizontal and vertical seismic response at a ridge of monoclinal slopes, which is half-space extensive, by taking into consideration vertical incident SH waves. The analytical model assumes the slopes are constituted by uniform viscoelastic material (damping = 1 %). The topographic amplifications factor in relation to the dimensionless frequency H/λ, where H is the relief height and λ is wavelength, confirms that greater amplification occurs at $H/\lambda = 0.2$. This corresponds to the topographic fundamental period $T_{fT} = 5H/V_S$ of the relief. Similar values of resonance were found by Paolucci (2002); however slightly lower values were also shown for high frequencies. In addition, in relation to the slope angle i, the $A_T H/\lambda$-depending curves decrease showing greater values for $i = 90°$ ($A_T \approx 1.5$), while they are lower for $i \leq < 30°$ ($A_T < 1.10$) and negligible for $i = 15°$. Similar values were obtained for the same relief model by Nguyen et al. (2013).

In natural complex topographic zones, Maufroy et al. (2012) used a three-dimensional numerical simulation code in order to investigate topographic effects, in some assigned points, assuming a multi isotropic source of seismic waves propagating in a complex 3-D media with a realistic surface topography. Their results showed topographic amplification factors up to 3.6 with a typical value range of 1.5–2.5 at the crests. However, the 3-D topographic amplification seems to be the combined result of lithological and geometric factors in which the pure topographic effect is difficult to fully quantify in numerous cases (Gallipoli et al., 2013). In addition, in some cases, recorded ground motions show a directionality in the resonance, (Bouchon et al., 1996; Spudich et al., 1996) encountering amplification values greater than the results formulated by the 2-D and 3-D numerical simulation models (Lovati et al., 2011). Furthermore, most comparison studies refer to noise or weak aftershock motions, and thus do not take into account or only slightly take into account the non-liner effect of system ridge-lithology (Gutierrez et al., 1992). On the other hand, the aforesaid studies have increased awareness in relation to the necessity to assess or predict topographic effect as a frequency depending variable and in an adequate way, in contrast with the simplistic models of the building codes. These models, in fact, provide the use of constant amplitudes in the entire spectrum, showing conditions of under-evaluation in several spectral ranges (Gallipoli et al., 2013; Barani et al., 2014).

1.3 Application scenarios

The SiSeRHMap was applied to a Synthetic Recurrent Scenario (SRS), a non-real area of 5 km^2 (2.5 km × 2.0 km) which is a synthetic reproduction of a common hilly scenery characterized by rigid/quasi rigid reliefs and a valley with soft lithologic units covering the bedrock (Fig. 1). The choice for using a SRS is based on the following reasons: (i) the possibility to simulate a vast number of sequences with different layer combinations in order to demonstrate the complete computational ability of the SiSeRHMap, (ii) the possibility to introduce different comparison scenarios, including also real scenerios, in the analysis, as shown in the topography amplification section (Sect. 4.2). The recognizing, consultation and interpretation of pre-existing data is a fundamental process in the definition of lithodynamic units and their spatial distribution (lithodynamic model). However, this preliminary process does not affect the performance of the code (therefore the methodology) but it affects the coherence of the results with the analysed area.

The input motion assumed in the simulation analysis is the same used by Grelle et al. (2014) in the real study area. It is a time-acceleration record that was spectrally-matched with the elastic spectrum design (with damping value of 0.05), which referred to the rigid site. The stratigraphic feature of the SRS (Fig. 1a) identified three cover lithodynamic units and two bedrocks, respectively rigid and non-rigid. The combination of these units determines the constitution of eight zones. The number and spatial distribution of the survey points are assumed coherent in the parametric characterization, and in the geometric features of the lithodynamic units, in reference to the simple subsoil setting of the SRS. However, in real case analyses and ignoring the ability of the modeller, the number, typology and spatial distribution of data must be taken into consideration in relation to the size and geological complexity of the area (Cardarelli et al., 2008), and also of the desired/required reliability degree.

The topographic feature (Fig. 1b) is characterized by a flat valley zone and a moderate high isolate relief with a slope angle of approximately 15–20° and values of curvature, at the ridge, of approximately 0.5. The resolution of the stratigraphic grid-data files and topographic grid-data is different, in order to respect the resolution expected by SiSeRHMap (see Sect. 4.2). The georeferenced coordinates of the input/output grid-data files locate the SRS in Southern Italy in an unreal way.

2 Gis Cubic Model: mod1 and mod2

The Gis Cubic Model (GCM) (Fig. 2) is a discretized and parametrized representation of an underground half-space that is capable of performing an overlay computation of geo-referenced grid data generated by common Geographic Information Systems platforms. This model intervenes in the SiSerHMap at two different and non-subsequent phases. In the first phase, the model parameterizes the lithodymamic units. In the second phase, the model produces seismic response maps. The GCM structure (Grelle et al., 2014) is based on a binary template matrix in which the rows (records) and columns (fields) represent respectively, the zones and layers. In the matrix, the presence or absence of the lithodynamic unit is defined in a binary way. The presence/absence of lithodynamic units is an exclusive propriety attributed to the covered layers. In contrast, the bedrock layer is always present at the base of the sequence. In this way, for a n layer sequence, the maximum number of possible zones is 2^{n-1}. The bedrock is the lithodynamic unit which is always present at the bottom of the sequence at the n-th layers and it can be defined as rigid or non-rigid, depending on whether the shear wave velocity is equal or greater to a prefixed value, $V_{S_{\mathrm{rig}}}$. Therefore, the condition

GMDD
8, 4487–4544, 2015

that the non-rigid bedrock must reach the $V_{S_{\mathrm{rig}}}$ value with a depth passing thus to the rigid condition is imposed; in this way a new lithodynamic unit up to the rigid bedrock is generated by the model. In SiSeRHMap, it is possible to consider the existence of two different bedrock typologies, thereby doubling the number of possible zones $(2 \cdot 2^{n-1})$ when this occurs.

2.1 Initial input data

In the GCM, the number of layers, and consequently the spatial extension of the lithodynamic units, are jointly defined by preparatory studies, as is the standard procedure in high levels of seismic microzonation. These studies are based on a preliminary collection of field surveys and pre-existing studies and datasets; subsequently, an accurate interpretation of geological, geotechnical and geophysical data permits the definition of both the typology and characterization (parametrization), as well as the spatial distribution, of the lithodynamic units.

The main focus in the parameterization of lithodynamic units is their spatial identification; this latter can be performed taking into account the lithology and their shear wave velocity–depth value distributions. In this way, to each lithodynamic unit is associated a layer in the GCM and it is defined by a linear-log or linear depending curve, V_S, z, which is identified by the intercept-velocity $V_{S_{0i}}$ and angular coefficient α_i. In some cases, this identification can show how the geophysical and geotechnical proprieties of soils can be decisive in the building of a GCM model. Therefore, the equations associated to the V_S, z lithodynamic unit distributions are:

(i) linear-log function for i-th covered layer,

$$V_{S_i}(z) = V_{S_{0i}} + \alpha_i \log(1+z) \tag{1}$$

(ii) linear function for non-rigid bedrock, nth layer

$$V_{S_n}(z) = V_{S_{0n}} + \alpha_n z; \quad \text{where } V_{S_{0n}} < V_{S_{\mathrm{RB}}} \tag{2}$$

(iii) constant value of shear wave velocity for rigid bedrock

$$V_{S_{0n}} \geq V_{S_{RB}}. \quad (3)$$

The curve fitting, and therefore the calibration of the parameters $V_{S_{0i}}$ and α_i, are obtained by means of the least-squares regression method. In relation to these aforementioned, the standard deviation permits evaluating the appropriate identification both in number and typology of the lithodynamic units (data and graphics in Supplement folder: OUTPUT\mod1_VsZ).

2.2 GCM frame

Input grid data files containing the thickness spatial distribution of the lithodynamic units, are necessary to instruct mod.2. These files are obtained via the common analysis that led to the definition of the lithodynamic units and zones. In fact, taking into consideration that the limit of a zone is also the extension line of at least one of the lithodynamic units, polyline features should define the minimum thickness as well as the borderline in the GIS pre-processing. In order to avoid computational bugs, the minimal thickness, $h_{(\mathrm{min})}$, of the lithodynamic units must not be zero. More specifically, this must correspond to the depth of the output of the desired seismic response, $z_{(\mathrm{out})}$. Figure 3 shows how the lithology with a thickness of less than $h_{(\mathrm{min})}$ did not identify the lithodynamic unit's presence; therefore, its spatial size must be preliminarily attributed to the nearest lithodynamic unit (above or below the non-identified lithodynamic unit).

Summarizing, the georeferenced grid input data is:

- Layer_1.txt, Layer_2.txt,... Layer_n-1.txt; extension of the covered layers in terms of one and zero values
- Bedrock_1.txt, Bedrock_2.txt (if this latter is present); extension of one or two bedrock typologies in terms of one and zero values
- Zones.txt, extension of zones, these are identified from a relative integer number.

- H_layer1.txt, H_layer_2.txt,...H_layer_n-1.txt; lithodynamic unit thicknesses obtained using appropriate GIS spatial interpolation techniques. For an adequate computational time, the grid-data resolution may be determined as follows:

$$\text{top resolution unit (m)} \approx \text{integer}\left(\sqrt{\frac{\text{surface (m}^2\text{)}}{10^6}}\right) \tag{4}$$

SiSeRHMap generates new "H_layer(i)_cor.txt" files in which the thicknesses less than $h_{(\min)}$ are reported as zero. In this way, the extension of the lithodynamic units is defined in relation to the map extension of the zones. (Some grid input files are reported in the Supplement folder: INPUT\GIS_in).

2.3 GCM for V_S, h trainer models

Once the V_S, z curves have been obtained, the binary template matrix has been inserted and the georeferenced grid files have been loaded, the GCM is thus structured and parameterized. In this phase, the GCM could start the mapped parameterization of the shear wave velocity for each layer as reported in Grelle et al. (2014). However in the SiSeRHMap, this computational process is performed in a subsequent second phase of the GCM (mod.5). In this first phase, the GCM gives data regarding the thicknesses range of the lithodynamic units in the zones to obtain the appropriate V_S, h trainer models reproducing the 1-D subsoil model in a dispersed way in the GCM. Therefore, the nature of the methodology requires that the equations which characterize and parameterize the GCM are equal to those that will be used in the generation of the V_S, h trainer models; thus, these equations will be subsequently circumstantiated, at a generic (x, y) geographic point, in the second phase of the GCM (GCM maps executor).

The V_S, h trainer models (Fig. 4) are defined by the subsequent equations (5 to 10) using the thickness values extracted, from the uniformly random distribution (Monte Carlo technique), within the maximum and minimum intervals found for each lithodinamic unit in each zone. The number of the models generated is freely chosen but it should be assumed taking into account thickness variability and the number of the lithodynamic units present in the zones (the default value is 10).

Therefore, once the GCM has been structured according to a (m x n) binary template matrix and the q number of the V_S, h trainer models has been established, mod.2 of the SiSeRHMap generates the V_S, h trainer models. In this way, the parameterization of an ith layer (i in [1, n]) in a jth zone (j in [1, m]) for a kth V_S, h trainer model (k in [1, q]) are defined by following points.

(i) The shear-wave velocity at the top and bottom of each $n-1$ cover layer is obtained using the parameterized log-linear functions; in relation to the combining of the layers position, the inversion of shear rigidity is also possible.

$$V_{S_{i(j,k)\mathrm{top}}} = V_{S_{0_i}} + \alpha_i \left\{ \log \left[1 + \left(\sum_{i=1}^{n-1} h_{i-1(j,k)} \right) \right] \right\} \tag{5}$$

$$V_{S_{i(j,k)\mathrm{bot}}} = V_{S_{0_i}} + \alpha_i \left\{ \log \left[1 + \left(\sum_{i=1}^{n-1} h_{i(j,k)} \right) \right] \right\} \tag{6}$$

(ii) With regards to the rigid bedrock, it is defined in relation to an established threshold of the shear wave velocity: $V_{S_{\mathrm{rig}}}$ (e.g. $V_{S_{\mathrm{rig}}} = 800\,\mathrm{m\,s^{-1}}$, EC8 prEN1998). In this way, the rigid bedrock is defined by a unique value of the shear-wave velocity $V_{S_{\mathrm{RB}}}$ with the condition that: $V_{S_{\mathrm{RB}}} \geq V_{S_{\mathrm{rig}}}$.

In contrast, when the bedrock is non-rigid (geological bedrock), the GCM automatically generates a new layer with a thickness of $h_{n(x,y)}$ and it assumes the n-th position while the rigid bedrock layer shifts to the $(n+1)$th position. The latter layer has a lithodynamic nature similar to non rigid bedrock but its depth confers to it the characteristics of rigid bedrock with a shear wave velocity equal to $V_{S_{\mathrm{RB}}}$. This condition is defined by the following equation:

$$V_{S_{n(j,k)\mathrm{bot}}} = V_{S_{\mathrm{RB}}} \tag{7}$$

GMDD
8, 4487–4544, 2015

thus it results that:

$$h_{n(j,k)} = \frac{\left(V_{S_{\mathrm{RB}}} - V_{S_{n(j,k)\mathrm{top}}}\right)}{\alpha_n}; \tag{8}$$

where

$$V_{S_{n(j,k)\mathrm{top}}} = \max\left(V_{S_{n-1(j,k)\mathrm{bop}}}; V_{S_{0n}}\right) \tag{9}$$

α_n is the gradient and the $V_{S_{0n}}$ is the intercept value relating to the V_S-depth regression linear curve of the non rigid bedrock (Eq. 2). In Eq. (8), when the max value is $V_{S_{n-1_{\mathrm{Bot}}}}$, it takes into account the possible increment of rigidity due to the lithostatic load of the upper cover layers; this case is manifested when the non-rigid bedrock shows relatively low values of the shear wave velocity in the V_S, z dispersion curve. In contrast, when the max value is $V_{S_{0n}}$, this indicates that the non rigid bedrock is near to the rigid condition and therefore it shows relatively high values of the shear wave velocity in the V_S, z dispersion curve.

(iii) The average shear-wave velocity of each lithodynamic unit is:

$$\overline{V}_{S_{i(j,k)}} = \frac{1}{2}\left(V_{S_{i(j,k)\mathrm{top}}} + V_{S_{i(j,k)\mathrm{bot}}}\right) \tag{10}$$

(iv) The fundamental vibration period is:

$$T_{f_{(j,k)}} = \frac{4\sum_{i=1}^{n} h_{i(j,k)}}{\sum_{i=1}^{n}\left(\overline{V}_{S_{i(j,k)}}\, h_{i(x,y)}\right) \Big/ \sum_{i=1}^{n} h_{i(j,k)}} \tag{11}$$

When the training model is composed only of the rigid bedrock (outcropping rock), the value of T_{f} is assumed to be 0.01 s.

GMDD
8, 4487–4544, 2015

A simulator for mapped seismic response using a hybrid model

G. Grelle et al.

3 Metamodeling: mod3 and mod4

The metamodel process is the core of SiSeRHMap; this process is composed of a semi-automated computation of the stratigraphic seismic responses of the V_S, h trainer models selected. Subsequently, a new robust and performing prediction model "Spectra" is trained on the spectral shape of these responses in order to emulate the stratigraphic seismic response in the succeeding GCM Maps Executor (mod.5)

3.1 Stratigraphic seismic response

The stratigraphic seismic response is performed in the SiSeRHMap by mod.3: Stratigraphic Response. Here, the dynamic site response is computed in a similar way to other computer program/codes: SHAKE (Schnabel et al., 1972; Idriss and Sun, 1992; Ordónez, 2003), EERA (Bardet et al., 2000), STRATA (Kottke and Rathje, 2008, 2010). The module computes the dynamic seismic response which refers to a one-dimensional soil column using a vertical linear wave propagation model which takes into consideration an equivalent shear-strain-dependent dynamic response of the soil-sequence. This method is commonly referred to as the viscoelastic equivalent linear analysis, in terms of total stress, taking into consideration a linear elastic bedrock. A horizontal polarized propagation of the shear waves through a site with infinite horizontal layers is assumed (Appendix A).

Despite the same computational performance of similar software (Fig. 5), mod.3 is dedicated to processing uploaded data from previous modules and subsequently returns data which is used in the next computational module (mod.4). Specifically, the Stratigraphic Seismic Response module performs an automatic computation of all the selected V_S, h trainer models. The natural unit weight, ρ, associated to each layering profile is empirically estimated in relation to the shear wave velocity. In this way, taking into account the low influence of this variable on the shear modulus due to its limited variation, the natural unit weight can be defined (Keçeli, 2012) as:

$$\rho = 4.4 V_S^{0.25} \tag{12}$$

Discussion Paper | Discussion Paper | Discussion Paper | Discussion Paper |

where ρ is expressed in $\mathrm{kN\,m^{-3}}$.

The input motion is considered on the outcropping to the rigid rock. Thereforeit is always deconvoluted within the sequence on the rigid bedrock (layer n or $n+1$), when the covered layers are present in the zone. The output response (Fig. 6) is provided at the outcropping of the surface detected by the assigned z_{out} depth; this surface is within the upper layer.

For each covered lithodynamic unit, as well as the non-rigid bedrock, the initial damping ratio, such as the strain-dependent values of normalized shear module and the damping ratio, must be inserted. From these latter values, the damping ratio and shear modulus degradation curves are obtained using the regression analysis in the $G(\gamma)/G_0$ and $D(\gamma)$ ratio curves fitting, which was introduced by Yokota et al. (1981) (Appendix A). Therefore, the computational iteration permits a convergence of both the equivalent calculated strain, $\gamma_{\mathrm{eq}} = (r \cdot \gamma_{\mathrm{max}})$ and the experimental strain, where γ_{max} is the maximum strain encountered in the dynamic time history, while r is the strain equivalent ratio; this can be freely assigned (the default value is 0.65) or it can be estimated in relation to a assigned earthquake magnitude, M, by the equation:

$$r = \frac{M-1}{10} \tag{13}$$

A number of iterations of 5 to 10 largely assures the convergence of a dynamic solution (the default value is: 10); in contrast the use of a number of iterations equal to zero entails a pure viscoelastic linear analysis. Nonetheless a constant value of the damping ratio is assumed for rigid bedrock. This value is attributed both to the fixed rigid bedrock and to the rigid bedrock resulting from non-rigid bedrock (the default value is: 0.01). For the zones characterized by outcropping rigid rock, the seismic response is automatically referred to the input motion.

In the Stratigraphic Response module, an additional module “View Signal” (Fig. 6) is associated in order to plot the time history signal (acceleration and strain) and spectra (transfer function, Fourier spectra, response spectra). (Some input and output files are reported in the Supplement folders: INPUT\Dynamic_properties; OUTPUT\mod3_Seismic_Response).

3.2 "Spectra": adaptive simulation model

Spectra, Σ, is a numerical adaptive model capable of emulating the theoretical stratigraphic seismic response. In this way, this model assumes a key role promoting the hybrid evolution of the procedures in SiSeRHMap.

The Spectra model is hither introduced and it stems from the previous experience of Grelle et al. (2014) in which hypotheses relating to the behaviour assumed by combinations of multi-parametric functions were introduced with the aim of obtaining good performances in the fitting of the acceleration response spectra. In Spectra, the natural influence on the spectral-trends of some main physical parameters are largely taken into consideration, confirming previous studies regarding Principal Component Analysis (PCA). The physical parameters used as independent variables in Spectra are: (i) the average shear wave velocity of the near surface lithodynamic unit, $V_{S(\mathrm{up})}$, (ii) the elastic fundamental period of the sequence, T_f, and (iii) the period, T. Its analytical form is:

$$\Sigma = \frac{x_1}{V_{S(\mathrm{up})}(1 + x_2 T^2)} + K \frac{x_3^{T_\mathrm{f}\log(V_{S(\mathrm{up})})}}{\exp\left[(x_4 T_\mathrm{f} + x_5 T)^2\right](T_\mathrm{f} + x_6 T)^{x_7 \frac{T_\mathrm{f}}{\log(V_{S(\mathrm{up})})}}} \log(1 + T^2) + x_8 \frac{T_\mathrm{f}}{T\, V_{S(\mathrm{up})}^2} \tag{14}$$

in which $x1, \ldots, x8$ are the eight calibration parameters (coefficients) and K is the modal scaling factor. Spectra permits a unique solution for each zone; in this way, the parameter, T can be considered a fast-changing variable (spectral variable), whereas the $V_{S(\mathrm{up})}$ and T_f change in relation to the V_S, h profile model (local variables) and the aforementioned eight calibration parameters are constant coefficients (zone variables). For

GMDD
8, 4487–4544, 2015
A simulator for mapped seismic response using a hybrid model
G. Grelle et al.

zones with rigid rock outcrops, T_f assumes a value of 0.01 s and the $V_{S(\mathrm{up})}$ is set equal to the corresponding rigid bedrock.

The three component functions, summed to define Spectra (Eq. 14), have specific and different roles in the fitness performance of the model. To this regard, and considering Σ as being dependant on T, it is worth highlighting that: (i) the first component has the role of "bed function" because it is the platform of the other component functions due to the fact that it greatly controls the intercept at the zero-period (PGA) and the tail fitting values, (ii) the second component is the "modal function" that controls the fitting peak values in the modal shape, (iii) the third component is the "PGA-correction function" which corrects the initial values permitting a more accurate fitting of the PGAs. In the bed function, the intercept (PGA) is inversely dependent on $V_{S(\mathrm{up})}$, though an addition or subtraction, sign x_8-coefficient dependent, is specifically performed by the PGA-correction function. The latter, in relation to the trend shown between T_f and PGA in the seismic response of a specific zone, permits taking into account the possible known non linear effect to decrement the spectral values at high frequencies (low periods). The modal function is the core of the Spectra adaptive model. It is a exponential equation capable of reproducing a symmetrical/asymmetrical modal or subordinated bimodal shapes generally shown by acceleration seismic responses in a large spectral range (Fig. 7). The modal function, which combines the parameters $V_{S(\mathrm{up})}$ and T_f in a different way, permits a chasing of the various peak-trend distributions by zones as well as possible single spectral behaviours or possible non peak-trend conditions due to the different influences of the non-linear responses. The modal scaling factor, K, acts only on the modal function. It is usually assumed to be equal to 1.00 and can be changed after calibration in order to scale the peaks.

In mod.4 of SiSerHMap, Spectra is trained on the theoretical spectra response values (mod.3) which are sampled starting from an initial period value of 0.001 s (PGA) and continue with regular sampling within the chosen spectral interval. The initial period value is fixed, while the sample rate (the default value is 0.1 s) and the number of samples (the default value is 15), and therefore the spectral interval, can be introduced

GMDD
8, 4487–4544, 2015

by the operator. The choice of the aforementioned values is fundamental since these define the efficacy and congruence of the metamodel. In addition the window sampling establishes the periods for which the seismic response maps will be returned which, in turn, will influence the design spectral maps. Taking into account that the sampling interval is equal for all the zones, this should include the whole spectral energy part without exceeding in the sampling of the spectral tail. In fact, the performance of fitness on the energy spectral part can be weak when a high number of tail values is involved. The training of Spectra aims at finding the optimized solution for the eight calibration parameters (Appendix B). It is performed by a nearing solution process by means of a dedicated Evolutionary Algorithm (EA) and a final optimizer algorithm: the Levenberg–Marquardt Algorithm (LMA). The latter is a curve-fitting algorithm used in many software applications for solving generic inverse problems.

The EA is a meta-heuristic method based on an evolutionary elitism of the offspring solutions that mutate up to satisfying or converging into a predefined fitness condition. The fitness of the solutions is defined by the fitting error which is expressed in terms of a mean square error (MSE). The EA is constituted by two breeding levels. In the first level, the offspring solutions are generated according to a corresponding Gaussian distribution in which the mean values representing the initial guesses population (low range parental) and corresponding standard deviations are supplied. In an iterative way, in the first level, only the population of offspring solutions which shows a fitness better than the previously encountered solutions, is permitted by passing to the second level in accordance with the elitism process. The number of procreations is four (fixed) and for each successive generation the probable parental affinity is increased (Appendix B). The elitism process is reset (mass extinction) when an assigned number of population solutions is reached and the convergence has not been reached yet. The convergence event occurs when an incremented assigned initial (minimum) error target E_{targ} is found. This error is increased by a assigned ratio (the default value is 0.01) at the end of the second breeding level when the process returns to the first breeding level. The assigned value of the initial error target depends on the shape of

GMDD
8, 4487–4544, 2015

the training seismic response curves in reference to the shape ability of the Spectra model. However the fitting and consequently the E_{targ} value can be dependent on the number of the randomly selected models, Nm, and on the number of the lithodynamic units present in the sequence, Nl. Taking into account this aspect, the default values of E_{targ} are empirically defined, for each zone, as follows:

$$E_{targ} = \frac{(\mathrm{Nm} \cdot \mathrm{Nl})}{1000} \tag{15}$$

The choice of an appropriate E_{targ} avoids a long computational time or, in contrast, the occurrence of premature convergences.

Optionally, in the metamodel module (mod4), it is possible to select the zone where an additional computation of "refinement" can be performed. This re-processing may be run when the fit or the shape regression curves are not considered satisfactory by the operator. The new processing can be performed using the initial guess parameters obtained in the previous processing and new standard deviation values, as well as a new lower E_{targ}, can be assigned.

4 GCM maps executor: mod.5

The maps executor is the second phase of the GCM and the last module of the SiSeRHMap. In this phase, the GCM module generates the hybrid stratigraphic seismic response maps (Fig. 8) after having further parameterized the model using data developed by the previous modules and some new inserted data. Therefore, a hybrid seismic response (HSR) can be computed both in reference only to the stratigraphic seismic response or also taking into account the topographic amplification effect. Data in relation to the latter is computed by an ancillary sub-module: "topographic amplification" that requires new geo-referenced topographic data files. Finally, an additional ancillary sub-module, the "design spectra", permits the computation of the damped synthetic design response spectra that envelopes the seismic response spectra using

GMDD
8, 4487–4544, 2015

the composed functions with shapes in accordance with EC8 and FEMA. (Some grid output files are reported in the Supplement folder: OUTPUT\GIS_out)

4.1 Stratigraphic seismic response mapping

For every geographic x, y point, the GCM is able to associate a corresponding j-zone and consequently also the relative parameters, processes, and information deriving from the previous modules. In this second phase, the GCM proceeds to configure itself using the common physic bases and hypothesis assumed in the construction and parameterization of the trainer V_S, h profiles (Sect. 2.3). These are as follows:

i. The average shear wave velocity, $\overline{V}_{S_{i(x,y)}}$, of the lithodynamic units, which is computed in accordance with Eq. (10); it assumes a value of zero where the lithodynamic is not present in the layer. In addition, if non-rigid bedrock is present at the bed of the sequence, the GCM generates the n-cover layer in which the $h_{n(x,y)}$ and $V_{S_{n(x,y)}}$ are defined in accordance with Eq. (9).

ii. The fundamental period $T_{f_{(x,y)}}$ is computed in accordance with Eq. (11). In addition, where the rock is outcropped the fundamental period assumes a value of 0.01 s.

iii. In each zone, the GCM recognizes the average shear wave velocity of the nearest surface lithodynamic unit $V_{S_{\mathrm{up}(x,y)}}$.

Once the GCM is parameterized, it is able to define the hybrid stratigraphic seismic response (Fig. 8) by solving the numerical model Spectra (Eq. 14) that in this context assumes the form:

$$\Sigma(T)_{(x,y)} = f\left[(T),(V_{S_{\mathrm{up}(x,y)}},T_{0_{(x,y)}}),((x_1)_j\ldots(x_8)_j)\right] \quad (16)$$

where the period T assumes the values in the spectra interval for which Spectra has been trained. The GCM maps executor computes the hybrid seismic response using the same period used in the metamodel training.

The maps of hybrid stratigraphic response (Fig. 8) can be affected by a quick change of data near the border of the zones; this effect can be due to the different fitting performed by the metamodel calibration as well as the geometrical cutting of the thickness discussed in Sect. 2.2. In order to take into account these affects, SiSerHMap permits the use of spatial Gaussian smoothing.

4.2 Topographic amplification mapping

Based on pre-existing studies and simulations on the effects of topographic amplification on seismic motion (Geli et al., 1988; Ashford et al., 1997; Maufroy et al., 2012, 2015), a prediction model has been developed. This model aims at predicting the spatial amplification effect on the seismic response of reliefs considering them to be constituted by a uniform material. To this scope, digital topographic attributes are used to introduce morphometric variables into the model. These are: (i) Digital Elevation Model, DEM (DTM_30.txt), (ii) Slope angle, i (Slope_30.txt), which is the arctangent of the first derivate of the DEM and (iii) Curvature, c (Curvatuere_30.txt), which is the second derivative of the DEM. The latter, is the inverse of the ray curvature which is expressed in terms of a resolution unit ratio. Therefore, a positive value of the curvature represents convex features such as ridges or edges, while a negative value indicates concave features such as a valley. A geometric trend of the curvature and slope along a typical profile relief (the upper part of Fig. 9) illustrates that the curvature assumes a greater value on the ridge, where the slope is minimum or near to zero, and the curvature assumes a zero value where the slope angle is greater. Towards the valley, the slope angle decreases while the curvature assumes negative values down to the minimum.

On the aforesaid bases, the prediction model of topographic amplification is a spatial-frequency dependent model constituted by a combination of the two sub-models (the lower part of Fig. 9). Taking into account a generic (x, y) point, A_{Tc} is the prediction model for the topographic amplification in ridge/edge regions:

$$A_{\mathrm{Tc}} = 1 + c\eta_t e^{-2\eta_t} + A_1 c\eta_t^2 e^{-A_2\eta_t^2} + A_3 c\eta_t \tag{17}$$

and A_{Ts} is the prediction model for the topographic amplification along the slope surface

$$A_{\mathrm{Ts}} = 1 + \left\{ r_H \left[\left(1 + \frac{B_1 c}{2\sqrt{\pi}} e^{-B_2\eta_t^2(1+c)} + B_3 \log \eta_t \right) (1 + \sin^2 i) \right] - r_H \right\} \tag{18}$$

where $r_H = H/H_{\mathrm{R}}$ and it is the relief ratio in which H and H_{R} are respectively the local slope height and the relief height, both of which are taken into consideration by the Basal Surface of Relief (BSR) where $H = 0$. A_1, A_2, A_3 and B_1, B_2, B_3 are the calibration parameters defined on the results obtained by the numerical model analysis of the 2-D homogeneous relief (discussed below in this section.) Hence, the dimensionless frequency, defined as slope height/wavelength, is:

$$\eta_t = \frac{H}{V_{S_{\mathrm{Reg}}} T} \tag{19}$$

where the $V_{S_{\mathrm{Reg}}}$ is the regional shear wave velocity. Finally, the topographic amplification A_{T} is the maximum value of A_{Tc} and A_{Ts} for each (x, y) point.

SiSeRHMap permits the definition of the BSR in relation to features of the topographic area (Appendix C), while the regional shear wave velocity must be assigned. This represents the average shear wave velocity of the rigid material constituting the relief/s, that can be different (frequently greater) to the shear wave velocity of the rigid bedrock assumed in the stratigraphic response analysis.

In general terms, the behaviour of the A_{Tc} and the A_{Ts} depend on the curvature and on the slope angle topography attributes which, in turn, depend on the value of the spatial resolution unit. In order to take into account this feature, the prediction models are calibrated on grid curvature data related to the spatial resolution unit of 30 m, which can be one order of magnitude higher than the resolution unit of the stratigraphic response (Eq. 4). This assumption gives the possibility to exclude the natural ripples of the slope which can be confused with ridges by the computational algorithm; in addition it is promoted by the fact that the amplification of low rigid ridges (height less than 30 m) occurs in frequencies with low interest for the buildings. The algorithm necessitates a recognition of the complete topographic features of the region considered in the stratigraphic response analysis; in some cases, this aspect involves taking into consideration an area much larger than one object of the stratigraphic response analysis. Subsequently, the algorithm performs an extracting, a georeferencing and a resolution adaptation to the smaller target area corresponding to the stratigraphic response area (e.g. in Fig. 11)

The A_{Tc} and A_{Ts} prediction models (Eqs. 17 and 18) are devised in a frequency dependant manner and calibrated in amplitude taking into account the findings and results derived from several simulation analyses based on physical models. Therefore, from these latter, the following calibration parameters result (Eqs. 17 and 18) as being $A_1 = 70$, $A_2 = 40$, $A_3 = 0.25$ and $B_1 = 3.60$, $B_2 = 3.24$, $B_3 = 0.12$. With regards to the modeling and calibration of A_{T}, Fig. 10 shows a geometrical model, similar to that considered by Geli et al. (1988), with a typical shape of the isolate relief of a middle-high altitude area (hilly areas). In this setting, a curvature of 0.5 is associated to the ridge, while the maximum of the slope angle of 30° is reached at midpoint of the relief. As illustrated, the topographic prediction models are nevertheless devised to provide amplified or non-amplified responses; consequently, they do not include spectral de-amplification (predominant in the valley), but they provide the peak values near to the topographic fundamental period of the relief. In addition, the A_{Tc} model provides the peak and it is predominant on the curvature zone (e.g. ridge or topographic border), while the A_{Ts} model is predominant along the slope, as expected. This last model defines the amplification curve for high periods, in all the cases.

For some corresponding positions along the surface of the relief, the comparison with the numerical simulation performed by Geli et al. (1988) shows (Fig. 11) that the topographic prediction model, A_T, is able to perform an adequate and efficient overlap, such as in comparison to the topographic edge feature (Ashford et al., 1997).

Bearing in mind that the strong natural spatial changing of the topographic attributes (mainly curvature) influences the efficacy of the model, some tests were performed on real areas in order to verify predictions on hilly-mountain real natural scenarios (Fig. 12). The results of the tests, show a substantial agreement with the 3-D numerical simulations (Maufroy et al., 2012, 2015) performed on a zone with a similar topographic feature; therefore the opportunity to calibrate and verify the sensibility of the model, is also provided. Consequently, a computational optimization, mainly aimed at minimizing the unreasonable concentration of high values, was performed. These high values are caused by natural roughness as well as by an anomaly in the base-digital map. The computational optimization, of A_T in A_T^*,consists in the smoothed numerical bass-cut of the slope angle $< 15^\circ$, curvature < 0.1, $H_R < 30$ m; and a Gaussian smoothing of the input curvature grid-map using a standard deviation value of 10–20 resolution units.

4.3 Design spectra mapping

The design spectra are obtained by the envelopment of the hybrid seismic response (HSR) in observance of the synthetic spectra drawn by the discontinuous function which defines the elastic response in the Euro Code 8 as well as in the FEMA 356 (2000). The envelope technique hither used needs to take in account the discrete nature of the hybrid seismic response The technique (Fig. 13) consists in the following computational steps:

1. recognition of the period, T_p, showing the maximum value (peak) of the hybrid seismic response HSR_{max};
2. computation of the mean, M, of the HSR values which are greater than the intercept HSR_0 value at period $T = 0.001$ ($\approx$ PGA);

GMDD
8, 4487–4544, 2015

3. computation of the mean M_R and M_L of HSR values greater than M respectively to the right and left of HSR_{max}
4. in this way the characterized parameters of design spectra are:

$$a_0 = HSR_0; \tag{20}$$

$$f_0 = \frac{HSR_{max}}{HSR_0}; \tag{21}$$

$$T_B = T_p\left[1 - \left(\frac{M}{M_L}\frac{N_L}{N}\right)\right]; \tag{22}$$

$$T_C = T_p\left[1 + \left(\frac{M}{M_R}\frac{N_R}{N}\right)\right]; \tag{23}$$

$$T_D = 1.6 + (4HSR_0);$$

where the $N = (N_L + N_R)$ is the number of HSR values over the M, and N_L and N_R are the respective numbers of the values to the left and right, excluding the HSR_{max}, in counting.

5 Discussion

SiSeRHMap algorithm is composed of interdependent computational modules and, in turn, of sub-models where each module can assume a more or less crucial role in the prediction and therefore in the expected performance. However, some simplification assumptions hither used are common to those used in simulation analysis performed by classic pure physically based methods. Among these assumptions, there is the necessity to use a simplified geometrical model of the subsoil as well as the necessity to parameterize it by means of the interpretation and spatial distribution of the local data

GMDD
8, 4487–4544, 2015

from field and/or laboratory surveys in order to define the lithodynamic model. In this contest, the hybrid model of SiSerHMap aims at providing an adequate computational method which combines satisfactory performance with a high computational discount. The current version of SiSerHMap is suitable for use in hilly and low-mountain zones which are mainly characterized by a non-complex stratification of the cover lithodynamic units.

A comparison between a SiSerHMap and a physically based numerical analysis code was performed. The Quake/W (GeoStudio, 2007) is a two dimensional geotechnical finite element (FEM) software which considers dynamic shear-strain-dependent viscoelastic material using dynamic linear equivalent analysis. This software offers the possibility to be parameterized using some input of SiSeRHMap: the shear modules increase with effective vertical stress and consequently with depth; in addition it gives the possibility to assume the equivalent shear strain ratio in relation to magnitude. The comparison (Fig. 14) regards six points distributed along cross section A (trace in Fig. 1) in order to investigate different lithologies and topographic features. The input earthquake used in the comparison analysis is the same used in the Stratigraphic Response module (mod.3). This input motion is properly scaled in order to produce in the check point a spectrum coherent with the deconvoluted 1-D spectrum at the same depth. The check point is placed under the covered layer in the flat zone, while the mesh is assumed with different dimensions in relation to the thickness of the layers.

The comparison analysis highlights how the hybrid response is close in amplification as well as coherent in frequency to the response provided by exclusively physically based models solved by the 2-D FEM-code. In this way, the aptitude of the hybrid model of SiSeRHMap seems to have a good compromise both for the definition of theoretical analytical response and for satisfying the exigency to provide the synthetic spectra shape required by building design. SiSeRHMap bases its uniqueness of analysis and high performance on the customized training process of the Spectra numerical model on local theoretical cases of stratigraphic seismic response. In this current version, the topographic amplification model is taken into account via the prediction model, too. Consequently, the design spectral parameters derived from the envelopment of the hybrid response are thus equipped with robust and accurate prediction as well as giving the advantage of mapped consultation.

6 Conclusion

The SiSeRHMap algorithm introduces a new method, defined as "hybrid", which is capable of creating maps of seismic response based on concepts of simulation cases, training and prediction.

The simulation (from mod1 to mod3) involves physic-numerical analysis consisting in a 1-D seismic response (mod.3), based on a linear-equivalent shear stress–strain model; this model performs on V_S, h profiles uniformly sampled in the GCM. The latter, in the first phase, is a structured-synthetic representation of the subsoil by layered lithodynamic units (mod.1 and mod.2). The training is the core of the method due to the fact that it provides its hybrid evolution in the stratigraphic seismic response. In this way, the adaptive prediction model Spectra seems to show robustness and efficacy features, while its accuracy is assured by the dedicated Evolutionary Algorithm (mod.4). The second phase of the GCM (mod.5) provides the mapped-solution of the Spectra model and the Topographic prediction model, in order to produce map sets of hybrid seismic responses and their envelopment process with the design spectra. Therefore, the general model at the base of SiSeRHMap confers to it the attribute of a first computational program that associates consolidated techniques of stratigraphic seismic response with advanced techniques regarding numerical emulation models and their training. In this way, SiSeRHMap permits the obtainment of map-data which can be easily diffused and consulted.

In this first version, SiSeRHMap focuses its action on the seismic response mainly characterized by stratigraphic and topographic effects. However, the possibility, to use digital morphological, lithological and water table distribution data by the GSM, permits

Discussion Paper | Discussion Paper | Discussion Paper | Discussion Paper |

GMDD

8, 4487–4544, 2015

A simulator for mapped seismic response using a hybrid model

G. Grelle et al.

conferring to SiSeRHMap large margins of evolution in the prediction of the amplification effects of buried valleys, as well as liquefaction and landslide phenomena.

Appendix A

Stratigraphic seismic response module

Module three computes the dynamic seismic response for a site-model with infinitely extended horizontal covered layers assuming a vertical propagation of polarized shear waves coming from a viscoelastic rigid bedrock (Fig. 1a). The non-linear viscoelastic strain that depends on the dynamic behaviour of soils constituting the covered layers is computed using the equivalent linear-viscoelastic analysis. Here, the base assumption is the one dimensional linear viscoelastic propagation of the shear wave in a homogeneous soil that is assumed as a Kelvin–Voigt solid in which the dynamic response is modelled using purely elastic spring and a purely viscous dashpot (Kramer, 1996). For this model, the solution to the harmonic wave with frequency, ω, provides displacement, u, as a function of depth, z, and time, t (Kramer, 1996), is:

$$u(z,t) = X \exp[j(\omega t + k^* z)] + Y \exp[j(\omega t - k^* z)] \tag{A1}$$

where the first and second terms represent the incident and reflected wave travelling; therefore X and Y are respectively the amplitudes of the incident wave in the negative z direction (upward) and reflected wave in the positive z direction (downward). In addition, in Eq. (A1), k^* is the complex wave number related to the complex shear modulus, G^*, damping ratio, D, and mass unit weight, ρ, of the soil, with:

$$k^* = \frac{\omega}{V_S^*} = \frac{\omega}{\sqrt{\frac{G^*}{\rho}}}, \tag{A2}$$

GMDD
8, 4487–4544, 2015

taking into consideration that the critical dumping ratio, D, is related to the viscosity, η, by:

$$\omega\eta = 2GD \tag{A3}$$

Here, it is reasonable to assume that the dynamic parameters G and D are almost constant in the frequency range where the analysis is usually performed. Hence, it is possible to express the complex shear modulus in terms of the critical damping ratio instead of the viscosity:

$$G^* = G + j\omega\eta = G\left(1 - 2D^2 + j2D\sqrt{1 - D^2}\right) \cong G(1 + 2jD) \tag{A4}$$

where G can be taken as being independent from frequency.

Hence, from Eq. (A1), for the top and bottom interfaces of the i layer with a thickness h_i (Fig. 1a), it is possible to express the strain $[(u_i(0,t),\ u_i(h_i,t)]$ in relation to the shear stress $[(\tau_i(0,t),\ \tau_i(h_i,t)]$ in this way:

$$\begin{aligned}\tau_i(z,t) &= (G_i + j\omega\eta_i)\frac{\delta u_i}{\delta z}\\ &= jk_iG_i\left\{X\exp\left[j\left(\omega t + k_i^* z\right)\right] + Y\exp\left[j\left(\omega t - k_i^* z\right)\right]\right\}\exp(j\omega t)\end{aligned} \tag{A5}$$

Therefore, imposing the continuity condition in the interface, in generic time, t, the following occurs:

$$u_i(h_i) = u_{i+1}(0) \quad \text{and} \quad \tau_i(h_i) = \tau_{i+1}(0) \tag{A6}$$

obtaining the relations:

$$X_i\exp\left(jk_i^*h_i\right) + Y_i\exp\left[-\left(jk_i^*h_i\right)\right] = X_{i+1} + Y_{i+1} \tag{A7}$$

$$k_i^*G_i^*\left\{X_i\exp\left(jk_i^*h_i\right) + Y_i\exp\left[-\left(jk_i^*h_i\right)\right]\right\} = k_{i+1}^*G_{i+1}^*(X_{i+1} + Y_{i+1}) \tag{A8}$$

GMDD
8, 4487–4544, 2015

For this later relation it is possible to express:

$$\alpha_i = \frac{k_i^* G_i^*}{k_{i+1}^* G_{i+1}^*} \equiv \sqrt{\frac{\rho_i G_i^*}{\rho_{i+1} G_{i+1}^*}} \tag{A9}$$

and therefore to define the following recurrence formulation:

$$X_{i+1} = \frac{1}{2}\left[X_i(1+\alpha_i)\exp\left(jk_i^* h_i\right) + Y_i(1-\alpha_i)\exp-\left(jk_i^* h_i\right)\right] \tag{A10}$$

$$Y_{i+1} = \frac{1}{2}\left[X_i(1-\alpha_i)\exp\left(jk_i^* h_i\right) + Y_i(1+\alpha_i)\exp-\left(jk_i^* h_i\right)\right] \tag{A11}$$

At the top of the first layer in the free surface condition the shear strength is $\tau_1(0) = 0$. Hence, Eq. (A5) defines that the amplitude of incident X_1 and reflect Y_1 waves are equal. Therefore, once the shear module and damping in each layer is known, it is possible to compute the value of generic X_i and Y_i within the sequence for an assigned range of frequency. The computation is performed assuming the iterative recursive calculation starting from the free surface where $X_1 = Y_1 = 1$ until the input (base) layer is reached. In this way, the transfer function for the incident and refract component of motion on the surface of the i layer can be obtained from equations:

$$X_i = x_i(\omega)X_1 \tag{A12}$$

$$Y_i = y_i(\omega)Y_1 \equiv y_i(\omega)X_1 \tag{A13}$$

Using Eq. (A1), the above transfer functions permit expressing the ratio of the amplitude of the harmonic motion in terms of displacement, velocity and/or acceleration between two layers for each frequency assumed. Therefore, the resultant transfer function, $\mathrm{TF}(\omega)$ that defines the amplification between the rock surface associated to layer (n) and the up-surface of a cover layer (i) or within the generic cover layer (i), when a sub-layer division of the column is performed, is defined as:

$$\mathrm{TF}_{(n,i)}(\omega) = \frac{x_i(\omega) + y_i(\omega)}{x_n(\omega) + y_n(\omega)} \tag{A14}$$

GMDD
8, 4487–4544, 2015

The above equation takes into consideration the amplification in relation to the input motion associated to an outcropping rock (n layer) where $X_n = Y_n$. In order to take into account that the input motion is within a sequence at the base of the cover layer, a deconvolution operation must be performed. This operation assumes that the descending transfer function can be computed assuming that $X_n \neq Y_n$ at the base of the cover deposit. Hence, the transfer function between the upper surface of the layer or the sub-layer (i) and bedrock surface (n) is defined as:

$$\mathrm{TF}_{(n,i)}(\omega)_{\text{input within}} = \frac{x_n(\omega) + y_n(\omega)}{2x_n(\omega)} \cdot \frac{x_i(\omega) + y_i(\omega)}{x_n(\omega) + y_n(\omega)} \tag{A15}$$

In mod.3 of SiSeRHMap, Eq. (A15) is set for the computation of $\mathrm{TF}_{(n,i)}(\omega)$ between the outcropping layer at the z output surface and bedrock surface. In this way, the response at the z output surface is computed by multiplying the Fourier amplitude spectrum of the input rock motion by the transfer function:

$$\mathrm{OUTPUT}\,(\omega) = \mathrm{TF}_{(n,i)}(\omega) \cdot \mathrm{INPUT}\,(\omega) \tag{A16}$$

The Fourier amplitude spectra of the input motion is defined using the numpy.fft module in the scipy library that computes the one-dimensional n point discrete Fourier Transform (DFT) of a real-valued array by means of an efficient algorithm called the Fast Fourier Transform (FFT) (Cooley and Tukey, 1965), (Press et al., 2007). In addition, this module computes the inverse of the n-point DFT for a real input matrix.

In relation to the strain dependent dynamic properties of the material, in the non-linear analysis, it is essential to know the strain values assumed during the motion. In the equivalent non-linear analysis, the dynamic module and damping is selected in the relative dynamic curve as a function of the strain level reaching. This approach gives the possibility to use the transfer function for computing the shear strain, γ, which is calculated in the middle of layer; the shear strain transfer function amplifies the motion and converts acceleration into strain. In reference to the setting expressed by Eq. (A16), the shear strain transfer function is defined as:

$$(\mathrm{TF}_{(n,i)}(\omega))_{\mathrm{strain}} = \frac{\gamma(\omega,z)}{\ddot{u}_n(\omega)_{\mathrm{outcropping}}} = \frac{jk_i^*\left[X_i \exp\left(\frac{jk_i^*h_i}{2}\right) - Y_i \exp\left(-\frac{jk_i^*h_i}{2}\right)\right]}{-\omega^2(2X_n)} \tag{A17}$$

The strain Fourier amplitude spectrum is obtained applying the strain transfer function to the Fourier amplitude spectrum of the input motion. Consequently, from this spectrum, the time history strain is obtained using the Fourier time domain conversion. The level of the shear strain defined as equivalent to the dynamic effective strain is assigned in terms of ratio (equivalent shear ratio) in relation to the maximum shear strain.

The relationship between the equivalent strain obtained from Eq. (A17) and the dynamic shear strain dependent parameters assumed in the computation of Eq. (A15) entails that this latter is resolvable by exclusively using an iterative computation until the obtainment of a convergent solution starting from the assigned initial value of the damping ratio. Mod.3 fits the data set regarding the shear modulus G/G_0, damping ratio $D(\%)$ and their relative strains, γ, using the following regression curves proposed by Yokota et al. (1981):

$$\frac{G}{G_0} = \frac{1}{1+\alpha\gamma^{\beta}} \tag{A18}$$

$$D(\%) = D_{\max} \exp\left(-\lambda \frac{G}{G_0}\right) \tag{A19}$$

Equations (A18) and (A19) are the non linear log-ascending and log-descending curves, where α, β and after $D_{\max}$ are constant coefficients calibrated using the Levenberg–Marquardt Algorithm in the computer aided version (Levenberg, 1944; Marquardt, 1963).

The seismic response spectra are defined by means of the widely used Shock Response Spectra (SRS) algorithm, in which the seismic response spectrum is calculated using an acceleration time history as a common base input excitation to a serial array of Single-Degree-Of-Freedom (SDOF) systems. Each system is a damped harmonic oscillator characterized by mass, stiffness and damping. The damping of each system is commonly assumed. The natural frequency is an independent variable. Thus, the calculation is performed for an arbitrary number of independent SDOF systems, each with a unique natural frequency. The systems are considered to have no mass-loading effect on the base input excitation (Irvine, 2012 and 2013).

The calculation method is carried out in the time domain via a convolution integral taking into consideration a base excitation with a ramp invariant function derivation of the digital recursive filtering relationship; the seismic response spectrum is the peak absolute acceleration response of each SDOF system to the time history base input (Smallwood, 1980). In the Stratigraphic Response module the seismic response spectra function was developed starting from srs.py and using the tompy.py library module (Irvine, 2014).

Appendix B

Evolutionary algorithm

In the Metamodel module (mod. 4), the calibration of the Spectra numerical model is performed by using the preprocessing Evolutionary Algorithm (EA) and subsequent optimization of data by means of the Levenberg–Marquardt Algorithm (LMA) (Levenberg,1944; Marquardt, 1963).

The LMA is implemented in Scipy Python's library as a "minpack" subroutine (http://www.math.utah.edu/software/minpack/minpack/lmstr1.html). The LMA is a curve-fitting algorithm widely used to solve non-linear least squares problems. However, as for many optimizer algorithms, the LMA finds local minima, which is not necessarily the global minima or optimal minima. This problem is due to some known aspects: (i) the large number of parameters; in fact a large number of parameters increases the search-hyperspace dimensions and therefore a higher number of local minimum values are

GMDD
8, 4487–4544, 2015

developed, (ii) the parameters differ from each other by some orders of magnitudes, (iii) the slowed convergence when the least squared function is very flat and the global minimum is located in "narrow canyon". Therefore, the non-uniqueness of an inverse solution and slowness in convergence are very sensitive to initial guesses.

The EA (Fig. 1b) is an evolutionary computational meta-heuristic method that consists in two breeding levels in which the 1st level generates, starting from initial guesses parameters (grandparents values) the offsprings (parents solutions) which are naturally selected for breeding (evolution) in the 2nd level. Consequently, in this level, the next generations are reproductions in a new generation (fourth in SiSeRHMap) from better parents; these offsprings are no longer subjected to natural selection but a new form of elitism is carried out. Using the root mean squared error in the definition of fitness, the reaching of convergence between the fitting minimum error, E_{min}, and the increasing error target E_{targ}, determines the satisfaction of the algorithm termination criterion and an optimized minima error solution should be reached after having tried to escape the unsatisfactory local minima error solutions. The numerical parameters obtained in this way are the best initial guesses in the LMA optimize process.

In the 1st breeding level, the parent solutions $(x_{1,i},...,x_{8,i})$ are generated in a normal distribution from given mean values $(x_1,...,x_8)$, defined as grandparents, and standard deviation $(\delta_1,...,\delta_8)$. The grandparents values differ by up to three/four orders of magnitude and are the results of the sensitive analysis performed on many metamodel cases; these values are reported as default but they can be changed.

When the ith parent population is generated, its performance in fitness, E_i, is compared with the best performance of the previous parent populations defined by the minimum current error E_{min}, and with the current error target E_{targ}. If E_i is equal or less than E_{targ}, the problem is already solved in the first breeding level. This occurs when there is a premature convergence (Eq. 15), due to the assuming of a high value of the starting E_{targ}, or when indeed a good solution is found (rarely). However, if E_i is greater than E_{min}, the iterating process continues and a new parent population is generated; in contrast, if E_i is less than E_{min}, the parent population passes to the 2nd breeding level

GMDD
8, 4487–4544, 2015

and the E_{min} assumes the current E_i value. The current E_{min} values are kept until the assigned iteration value, B, is reached.

In the 2nd breeding level, the kth descending populations can be generated; starting from $k = 0$, j iterate solutions are procreated in normal distribution series assuming as mean values $(x_{1,j,0},\ldots,x_{8,j,0})$, that are the elect parent population $(x_{1,i},\ldots,x_{8,i})$ deriving from the 1st level, and standard deviation $(\delta_1,\ldots,\delta_8)$. The procreation of new j populations continues until a new better error is found or until an assigned j iteration value, C, is reached. In the first case, the population is a new generation and it assumes the role of kth procreator having mean values, $x_{1,j,k},\ldots,x_{8,j,k}$, and a standard deviation $\delta_1/k,\ldots,\delta_8/k$. The k iteration of the afore-mentioned loop continues up until an assigned number of generations, D, is reached; if the convergence is not found in this process, in addition to the reaching of C, the process returns to the 1st level and the error target is increased of A value. When the process returns to the 1st level, the minimum error assumes the value of the last minimum error found in this level. However, the minimum error and target error are reset when B in the i iteration value is reached.

The optimal solution does not contemplate absolute minimums, being that for one or more elements (inter-space vectors), the solution tends to be infinite. For this reason, a solution that gives values that do not exceed a greatness of 10^5, is considered optimal.

Appendix C

Topographic amplification

The SySeRHMap permits a definition of the Basal Surface of Relief (BSR) in relation to the general setting of the topographic area. A dedicated algorithm defines:

a. the BSR as a wary surface. The algorithm performs the numerical scanning in X and Y (East–West and North–South) directions choosing the maximum and minimum elevation value Ex_{max}, Ey_{max} and Ex_{min}, Ey_{min}. Therefore, taking into consideration the generic map position $(x, y) \in (X, Y)$ the height of the relief is defined as:

a1. $H = \min[(E_{x,y} - E_{x_{min}}), (E_{x,y} - E_{y_{min}})]$
$H_{max} = \min[(E_{x_{max}} - E_{x_{min}}), (E_{y_{max}} - E_{y_{min}})]$

a2. $H = \max[(E_{x,y} - E_{x_{min}}), (E_{x,y} - E_{y_{min}})]$
$H_{max} = \min[(E_{x_{max}} - E_{x_{min}}), (E_{y_{max}} - E_{y_{min}})]$

b. the BRS as a plain surface with elevation, E_{flat}, results from an average elevation of the flat zones. These latter are so defined when they show a slope $i < 5°$ and curvature $-0.05 \leq c \leq 0.05$.

b1. $H = E_{x,y} - E_{flat}$
$H_{max} = \max[(E_{x_{max}} - E_{flat}), (E_{y_{max}} - E_{flat})]$

Code availability

SiSeRHMap 1.0 is available at http://www.geosmartapp.it, where the trial version and the full version of the code were uploaded. The trial version is quickly available and it only permits the running of the application case reported in the manuscript. The full version is freely available on demand after inserting the password obtained by registration. In the folder of the code, the operator can also find the user guide and the input files that were used in the application case.

The Supplement related to this article is available online at doi:10.5194/gmdd-8-4487-2015-supplement.

Author contributions. The SiSeRHMap methodology was ideated by G. Grelle with the collaboration of L. Bonito. G. Grelle was also the developer and the project creator of the code source. L. Bonito provided support in the Geographic Information System and in the development of the Gis Cubic Model. A. Lampasi supported the planning of the Evolutionary Algorithm. P. Revellino and L. Guerriero collaborated in the definition of the Synthetic Recurrent Scenario (SRS) and in the Textual User Interface and manuscript editing. G. Sappa and F. M. Guadagno were research and project coordinators.

Acknowledgements. The PRIN 2010–2011 (project 2010E89BPY_001 to F. M. Guadagno) financed the cost for document editing of the application of the Patent methodology.

References

Ashford, S. A., Sitar, N., Lysmer, J., and Deng, N.: Topographic effects on the seismic response of steep slopes, B. Seismol. Soc. Am., 87, 701–709, 1997.

Assimaki, D., Kausel, E., and Gazetas, G.: Soil-dependent topographic effects: a case study from the 1999 Athens earthquake, Earthq. Spectra, 21, 929–966, 2005.

Athanasopoulos, G. A., Pelekis, P. C., and Leonidou, E. A.: Effects of surface topography on seismic ground response in the Egion (Greece) 15 June 1995 earthquake, Soil Dyn. Earthq. Eng., 18, 135–149, 1999.

Barani, S., Massa, M., Lovati, S., and Spallarossa, D.: Effects of surface topography on ground shaking prediction: implications for seismic hazard analysis and recommendations for seismic design, Geophys. J. Int., 197, 1551–1565, 2014.

Bardet, J. P., Ichii, K., and Lin, C. H.: EERA: a Computer Program for Equivalent-Linear Earthquake site Response Analyses of Layered Soil Deposits, Department of Civil Engineering, University of Southern California, Los Angeles, California, 2000.

Bianchi Fasani, G., Cavinato, G. P., Petitta, M., Scarascia Mugnozza, G., and Voltaggio, M.: The geological model of Celano town area for seismic microzonation activities, Soil Dyn. Earthq. Eng., 28, 978–985, 2008.

Borcherdt, R. D.: Estimates of site-dependent response spectra for design (methodology and justification), Earthq. Spectra, 10, 617–653, 1994.

Bouchon, M., Schultz, C. A., and Toksoz, M. N.: Effect of three-dimensional topography on seismic motion, J. Geophys. Res., 101, 5835–5846, 1996.

Cardarelli, E., Ceracato, M., de Nardis, R., Di Filippo, G., and Milana, G.: Geophysical investigations for seismic zonation in municipal areas with complex geology: the case study of Celano, Italy, Soil Dyn. Earthq. Eng., 28, 950–963, 2008.

Çelebi, M.: Topographical and geological amplifications determined from strong-motion and aftershocks records of the 3 March 1985 Chile earthquake, B. Seismol. Soc. Am., 77, 1147–1167, 1987.

Compagnoni, M., Pergalani, F., and Boncio, P.: Microzonation study in the Paganica–San Gregorio area affected by the 6 April 2009 L'Aquila earthquake (central Italy) and implications for the reconstruction (Article), B. Earthq. Eng., 9, 181–198, 2011.

Cooley, J. W. and Tukey, J. W.: An algorithm for the machine calculation of complex Fourier series, Math. Comput., 19, 297–301, 1965.

Del Gaudio, V. and Wasowski, J.: Directivity of slope dynamic response to seismic shaking, Geophys. Res. Lett., 34, L12301, doi:10.1029/2007GL029842, 2007.

Del Prete, M., Guadagno, F. M., and Scarascia-Mugnozza, G.: Earthquake induced damage in an historic area: the September–October 1997 seismic sequence which affected Assisi, central Italy, B. Eng. Geol. Environ., 57, 101–109, 1998.

Durand, S., Gaffet, S., and Virieux, J.: Seismic diffracted waves from topography using 3-D discrete wavenumber-boundary integral equation simulation, Geophysics, 64, 572–578, doi:10.1190/1.1444564, 1999.

Fan, F. M., Fleischmann, A. S., Collischonn, W., Ames, D. P., and Rigo, D.: Large-scale analytical water quality model coupled with GIS for simulation of point sourced pollutant discharges, Environ. Modell. Softw., 64, 58–71, 2015.

FEMA 356: Prestandard and Commentary for the Seismic Rehabilitation of Buildings, prepared by the Building Seismic Safety Council for the Federal Emergency Management Agency, 2000, Washington, D.C., 2000.

Gallipoli, M. R., Bianca, M., Mucciarelli, M., Parolai, S., and Picozzi, M.: Topographic versus stratigraphic amplification: mismatch between code provisions and observations during the L'Aquila (Italy, 2009) sequence, B. Earthq. Eng., 11, 1325–1336, 2013.

Ganapathy, G. P.: First level seismic microzonation map of Chennai city – a GIS approach, Nat. Hazards Earth Syst. Sci., 11, 549–559, doi:10.5194/nhess-11-549-2011, 2011.

Geli, L., Bard, P. Y., and Jullen, B.: The effect of topography on earthquake ground motion: a review and new results, B. Seismol. Soc. Am., 78, 42–63, 1988.

Grasso, S. and Maugeri, M.: The seismic microzonation of the city of Catania (Italy) for the Etna scenario earthquake ($M = 6.2$) of 20 February 1818, Earthq. Spectra, 28, 573–594, 2012.

Grelle, G. and Guadagno, F. M.: Regression analysis for seismic slope instability based on Double Phase Viscoplastic sliding model of the rigid block, Landslides, 5, 583–597, 2013.

GMDD
8, 4487–4544, 2015

Grelle, G., Revellino, P., and Guadagno, F. M.: Methodology for seismic and post-seismic stability assessing of natural clay slope based on a visco-plastic behavioural model in simplified dynamic analysis, Soil Dyn. Earthq. Eng., 12, 1248–1260, 2011.

Grelle, G., Bonito, L., Revellino, P., Guerriero, L., and Guadagno, F. M.: A hybrid model for mapping simplified seismic response via a GIS-metamodel approach, Nat. Hazards Earth Syst. Sci., 14, 1703–1718, doi:10.5194/nhess-14-1703-2014, 2014.

Gutierrez, C. and Singh, S. K.: Site effect study in Acapulco, Guerrero, Mexico: comparison of results from strong-motion and microtremor data, B. Seismol. Soc. Am., 82, 642–659, 1992.

Hashemi, M. and Alesheikh, A. A.: Development and implementation of a GIS-based tool for spatial modeling of seismic vulnerability of Tehran, Nat. Hazards Earth Syst. Sci., 12, 3659–3670, doi:10.5194/nhess-12-3659-2012, 2012.

Hassanzadeh, R., Nedović-Budić, Z., Alavi Razavi, A., Norouzzadeh, M., and Hodhodkian, H.: Interactive approach for GIS-based earthquake scenario development and resource estimation (Karmania hazard model), Comput. Geosci., 51, 324–338, 2013.

Hong, S., Yu, X., Park, S. K., Choi, Y.-S., and Myoung, B.: Assessing optimal set of implemented physical parameterization schemes in a multi-physics land surface model using genetic algorithm, Geosci. Model Dev., 7, 2517–2529, doi:10.5194/gmd-7-2517-2014, 2014.

Hough, S. E., Altidor, J. R., Anglade, D., Given, D., Janvier, M. G., Maharrey, J. Z., Meremonte, M., Mildor, B. S.-L., Prepetit, C., and Yong, A.: Localized damage caused by topographic amplification during the 2010 M7.0 Haiti earthquake, Nat. Geosci., 3, 778–782, 2010.

Idriss, I. M. and Sun, J. I.: User's Manual for SHAKE91, Center for Geotechnical Modeling, Department of Civil Engineering, University of California, Davis, 1992.

Irvine, T.: An Introduction to the Shock Response Spectrum - Revision S, Vibrationdata, available at: http://www.vibrationdata.com/tutorials2/srs_intr.pdf (last access: 11 June 2015), 2012.

Irvine, T.: Derivation of the Filter Coefficients for the Ramp Invariant Method as Applied to Base Excitation of a Single-Degree-of-Freedom System – Revision B, available at: http://www.vibrationdata.com/ramp_invariant/ramp_invariant_base.pdf (last access: 11 June 2015), 2013.

Irvine, T.: Vibration data Pyrotechnic Shock and Shock Response Spectrum Page, Vibrationdata, http://www.vibrationdata.com/SRS.htm (last access: 11 June 2015), 2014.

GMDD
8, 4487–4544, 2015

Jimenez, M. J., Garcia-Fernadez. M., Zonno, G., and Cella, F.: Mapping sol effects in Barcelona, Spain, through an integrated GIS environment, Soil Dyn. Earthq. Eng., 19, 289–301, 2000.

Kawase, H. and Aki, K.: Topography effect at the critical SV-wave incidence: possible explanation of damage pattern by the Whittier Narrows, California, earthquake of 1 October 1987, B. Seismol. Soc. Am., 80, 1–22, 1990.

Keçeli, A.: Soil parameters which can be determined with seismic velocities, Jeofizik, 16, 17–29, 2012.

Kienzle, A., Hannich, D., Wirth, W., Ehret, D. Rohn, J., Ciugudean, V., and Czurda, K.: A GIS-based study of earthquake hazard as a tool for the microzonation of Bucharest, Eng. Geol., 87, 13–32, 2006.

Kokošin, J. and Gosar, A.: Seismic microzonation of Breginjski Kot (NW Slovenia) based on detailed engineering geological mapping, Sci. World J., 2013, ID 626864, 12 pp., 626854, 2013.

Kolat, Ç., Doyuran, V., Ayday, C., and Lütfi Süzen, M.: Preparation of a geotechnical microzonation model using Geographical Information Systems based on Multicriteria Decision Analysis, Eng. Geol., 87, 241–255, 2006

Kottke, A. R. and Rathje, E. M.: Technical Manual for Strata, Report 2008/10, Pacific Earthquake Engineering Research [PEER] Center, Berkeley, California, 95 pp., 2008.

Kottke, A. R. and Rathje, E. M.: Strata, Neeshub, available at: https://nees.org/resources/strata (last access: 11 June 2015), 2010.

Kramer, S. L.: Geotechnical Earthquake Engineering, Prentice Hall, University of Washington, USA, 653 pp., 1996.

Lachet, C., Hatzfeld, D., Bard, P. Y., Theodulidis, N., Papaioannou, C., and Savvaidis, A.: Site effects and microzonation in the City of Thessaloniki (Greece) comparison of different approaches, B. Seismol. Soc. Am., 86, 1692–1703, 1996.

Lampasi, D. A., Podestà, L., and Carbone, P.: Synthesis of binary test sequences with good spectral properties using an evolutionary algorithm, Measurement, 39, 245–251, 2006.

Levenberg, K.: A method for the solution of certain problems in least squares, Q. Appl. Math., 2, 164–168, 1944.

Lovati, S., Bakavoli, M. K. H., Massa, M., Ferretti, G., Pacor, F., Paolucci, R., Haghshenas, E., and Kamalian, M.: Estimation of topographical effects at Narni ridge (central Italy): comparisons between experimental results and numerical modelling, B. Earthq. Eng., 9, 1987–2005, 2011.

Marquardt, D.: An algorithm for least-squares estimation of nonlinear parameters, SIAM J. Appl. Math., 11, 431–441, 1963.
Massa, M., Lovati, S., D'Alema, E., Ferretti, G., and Bakavoli, M.: An experimental approach for estimating seismic amplification effects at the top of a ridge, and the implication for ground-motion predictions: the case of Narni, central Italy, B. Seismol. Soc. Am., 100, 3020–3034, 2010.
Maufroy, E., Cruz Atienza, V. M., and Gaffet, S.: A robust method for assessing 3-D topographic site effects: a case study at the LSBB Underground Laboratory, France, Earthq. Spectra, 28, 1097–1115, 2012.
Maufroy, E., Cruz Atienza, V. M., Cotton, F., and Gaffet, S.: Frequency scaled curvature as a proxy for topographic site effect amplification and ground motion variability, B. Seismol. Soc. Am., 105, 354–367, 2015.
Milana, G., Azzara, R. M., Bertrand, E., Bordoni, P., Cara, F., Cogliano, R., Cultrera, G., Di Giulio, G., Duval, A. M., Fodarella, A., Marcucci, S., Pucillo, S., Régnier, J., and Riccio, G.: The contribution of seismic data in microzonation studies for downtown L'Aquila, B. Earthq. Eng., 9, 741–759, 2011.
Moscatelli, M., Pagliaroli, A., Cavinato, G. P., Castenetto, S., and Naso, G.: Seismic microzonation of Palladine Hill, Roman Forum and Coliseum Archaeological Area, B. Earthq. Eng., 12, 1269–1275, 2014.
Nath, S. K.: Seismic hazard mapping and microzonation in the Sikkim Himalaya through GIS integration of site effects and strong ground motion attributes, Nat. Hazards, 31, 319–342, 2004.
Nguyen, H. T., Fleurisson, J. A., and Cojean, R.: Evaluation of topography site effect in slope stability under dynamic loading, in: Vienna Congress on Recent Advances in Earthquake Engineering and Structural Dynamics, 28–30 August 2013, Vienna, Austria, 521, 10 pp., 2013.
NTC, Norme Tecniche per le Costruzioni: DM 14 Gennaio 2008, Gazzetta Ufficiale, n. 29 del 4 Febbraio 2008, Supplemento Ordinario n. 30, Istituto Poligrafico e Zecca dello Stato, Roma, available at: www.cslp.it (last access: 11 June 2015), 2008.
Ordónez, G. A.: SHAKE 2000: a Computer Program for the 1-D Analysis of Thegeotechnical Earthquake Engineering Problem, GeoMotions, avialable at: http://www.shake2000.com (last access: 11 June 2015), 2003.

Paolucci, R.: Amplification of earthquake ground motion by steep topographic irregularities, Earthq. Eng. Struct. D, 31, 1831–1853, 2002.
Papadimitriou, A. G., Antoniou, A. A., Bouckovalas, G. D., and Marinos, P. G.: Methodology for automated GIS-aided seismic microzonation studies, Comput. Geotech., 35, 505–523, 2008.
Pischiutta, M., Cultrera, G., Caserta, A., Luzi, L., and Rovelli, A.: Topographic effects on the hill of Nocera Umbra, central Italy, Geophys. J. Int., 182, 977–987, 2010.
Press, W., Teukolsky, S., Vetterline, W. T., and Flannery, B. P.: Numerical Recipes: the Art of Scientific Computing, chapt. 12–13, Cambridge Univ. Press, Cambridge, UK, 2007.
Reed, S. E., Boggs, J. L., and Mann, J. P.: A GIS tool for modeling anthropogenic noise propagation in natural ecosystems, Environ. Modell. Softw., 37, 1–5, 2012.
Rodríguez-Marek, A., Bray, J. D., and Abrahamson, N. A.: An empirical geotechnical seismic site response procedure, Earthq. Spectra, 17, 65–87, 2001.
Sánchez-Sesma, F. J.: Diffraction of elastic waves by three-dimensional surface irregularities, B. Seismol. Soc. Am., 73, 1621–1636, 1983.
Schnabel, P. B., Lysmer, J., and Seed, H. B.: SHAKE: a Computer Program for Earthquake Response Analysis of Horizontally Layered Sites, Report No. EERC 72–12, College of Engineering, University of California, Berkeley, CA, 88 pp., 1972.
Smallwood, D. O.: Improved recursive formula for calculating shock response spectra, Shock and Vibration Bulletin, Symp. on Shock and Vib., 51st; San Diego, CA, USA, 21–23 October 1980, 211–217, 1980.
Soares, J., Kousa, A., Kukkonen, J., Matilainen, L., Kangas, L., Kauhaniemi, M., Riikonen, K., Jalkanen, J.-P., Rasila, T., Hänninen, O., Koskentalo, T., Aarnio, M., Hendriks, C., and Karppinen, A.: Refinement of a model for evaluating the population exposure in an urban area, Geosci. Model Dev., 7, 1855–1872, doi:10.5194/gmd-7-1855-2014, 2014.
Sokolov, V. Y. and Chernov, Y. K.: Probabilistic microzonation of urban territories: a case of Tashkent City, Pure Appl. Geophys., 158, 2295–2311, 2011.
Spudich, P., Hellweg, M., and Lee, W. H. K.: Directional topographic site response at Tarzana observed in aftershocks of the 1994 Northridge, California, earthquake: implications for mainshock motions, B. Seismol. Soc. Am., 86, 193–208, 1996.
Todd, D. R. and Harris, J. R.: De facto microzonation through the use of soils factors in design triggers, in: International Conference on Seismic Zonation, 5th. Proceedings, 17–19 October 1995, Nice, France, Quest Editions, France, 510–517, 1995.

GMDD
8, 4487–4544, 2015

A simulator for mapped seismic response using a hybrid model

G. Grelle et al.

Title Page
Abstract | Introduction
Conclusions | References
Tables | Figures
◀I | ▶I
◀ | ▶
Back | Close
Full Screen / Esc
Printer-friendly Version
Interactive Discussion

Turk, T., Gümüşay, U., and Tatar, O.: Creating infrastructure for seismic microzonation by Geographical Information Systems (GIS): a case study in the North Anatolian Fault Zone (NAFZ), Comput. Geosci., 43, 167–176, 2012.

Wang, C., Duan, Q., Gong, W., Ye, A., Di, Z., and Miao, C.: An evaluation of adaptive surrogate modeling based optimization with two benchmark problems, Environ. Modell. Softw., 60, 167–179, 2014.

Yazdi, J. and Neyshabouri, S.: Adaptive surrogate modeling for optimization of flood control detention dams, Environ. Modell. Softw., 61, 106–120, 2014.

Yokota, K., Imai, T., and Kanemori, T.: Dynamic deformation characteristics of soils determined by laboratory tests, OYO Tec. Rep., 3, 13–37, 1981.

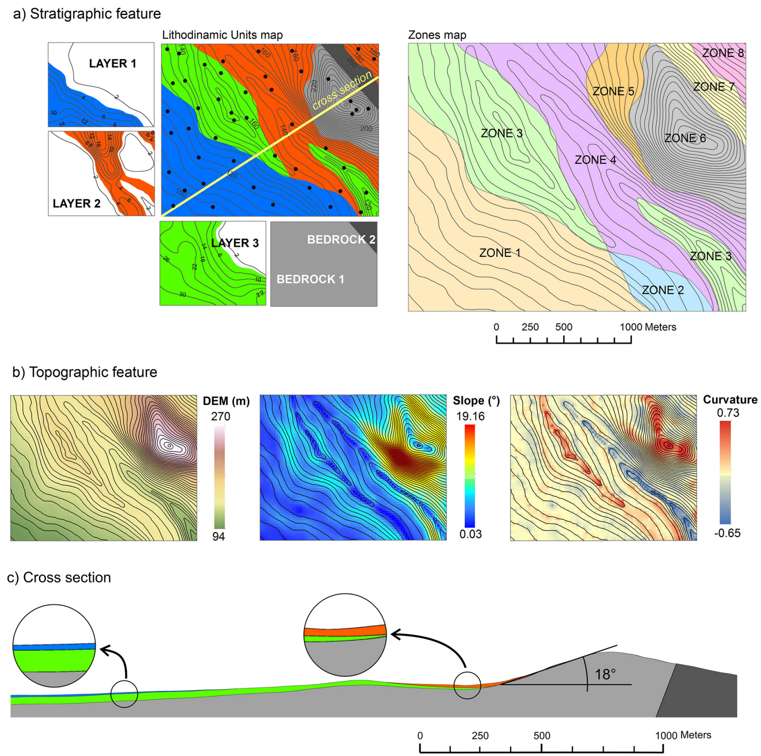

Figure 1. Synthetic Recurrent Scenery (SRS). **(a)** On the left: the maps with a resolution of 2.00 m regarding the covered layers and bedrock layers; for each covered layer, the iso-thicknesses of the relative lithodynamic unit, resulting from the interpolation of the hypothesized field survey is reported (black point in Lithodynamic Units map); the coloured polygon is the correct extension of the unit corresponding to an iso-thickness of 3.00 m (paragraph 2.2); on the right: the zones characterizing the SRSare shown; **(b)** topographic features in terms of the DEM (Digital Elevation Model), slope and curvature maps with a resolution of 30 m.

GMDD
8, 4487–4544, 2015

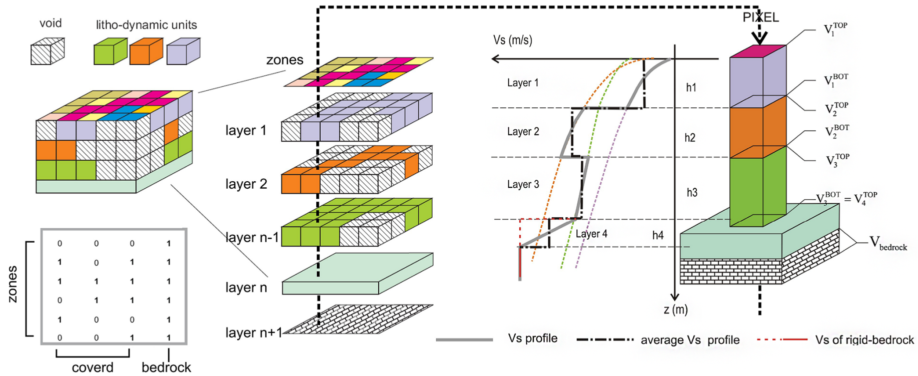

Figure 2. Subsoil half-space modeling by the GIS Cubic Model (GCM) and binary template matrix (e.g. referred to four layers, three covered layers and one non-rigid bedrock) and 1-D layered V_S, h profile deriving from the GCM computational analysis (figure from Grelle et al., 2014).

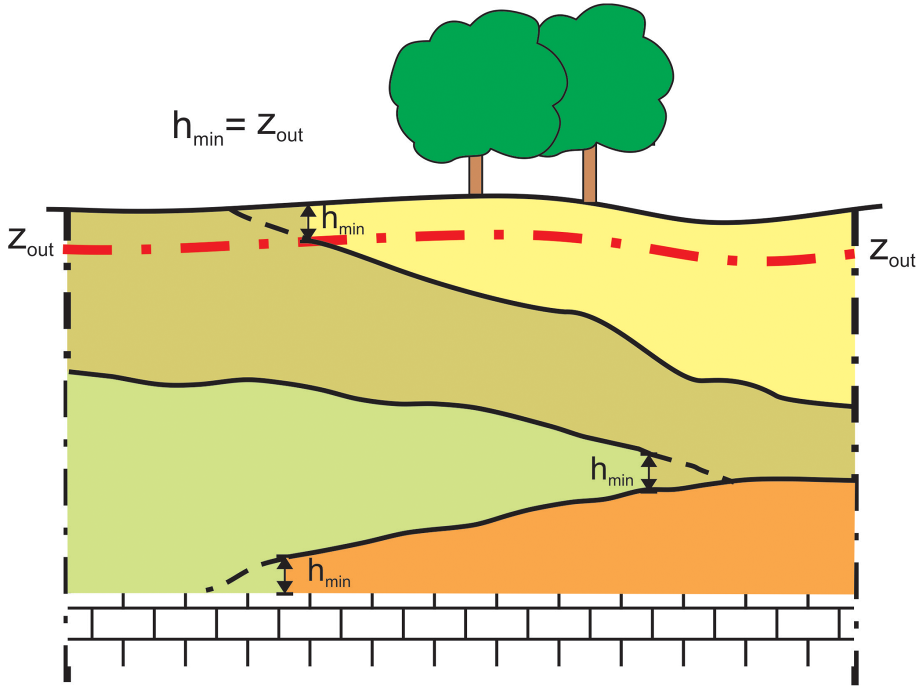

Figure 3. Example of the thicknesses cutting performed by mod2 of the SiSeRHMap.

GMDD
8, 4487–4544, 2015

A simulator for mapped seismic response using a hybrid model

G. Grelle et al.

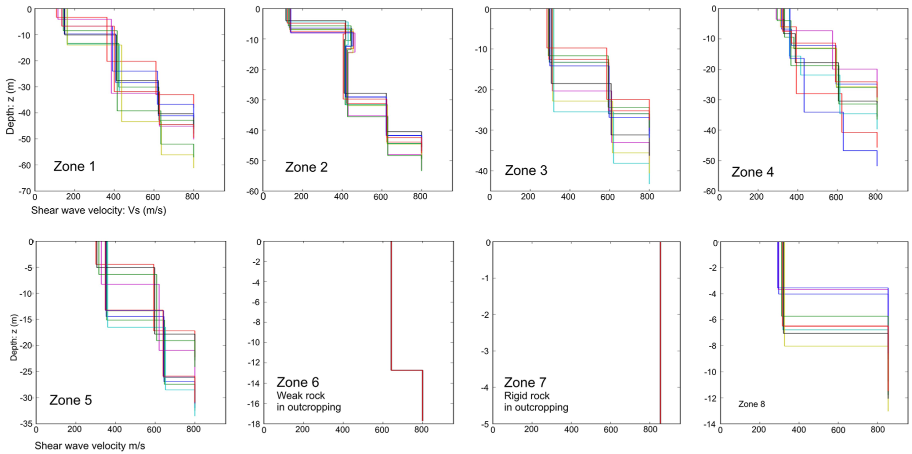

Figure 4. V_S, h trainer models: there are ten trainer models theoretically encountered in each of the eight zones which are presented in the SRS (Fig. 1a).

GMDD
8, 4487–4544, 2015

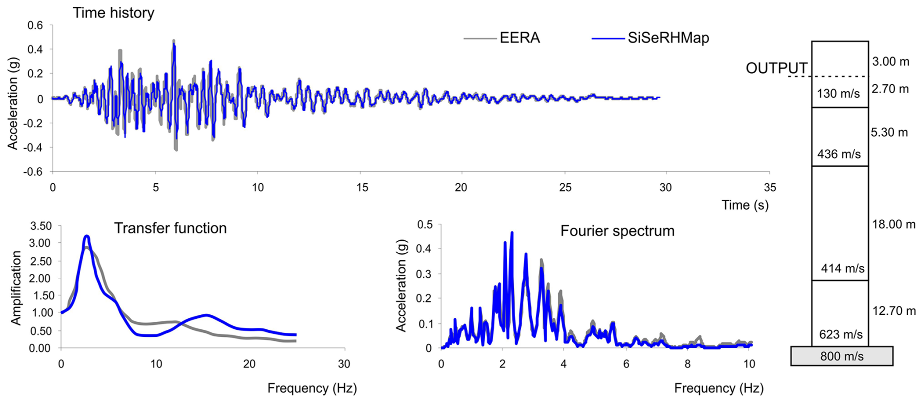

Figure 5. Comparison between EERA and SiSeRHMap (mod 3, Stratigraphic Response) on a 1-D model related to the 3rd trainer V_S, h model regarding zone 2.

GMDD
8, 4487–4544, 2015

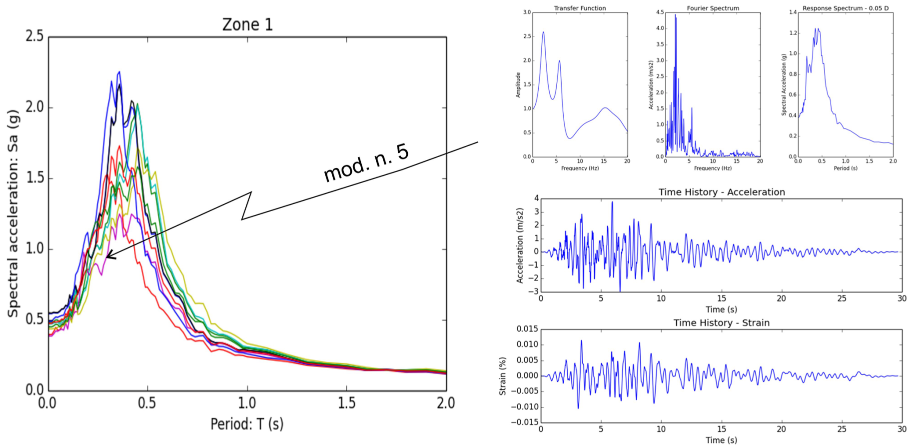

Figure 6. Example of the stratigraphic seismic response set of zone 1 with 0.05 damping; for this set, the graphics plotted of the signal view module related to the 5th trainer V_S, h model are also shown. In the analysis (all zones), the equivalent stress ratio is obtained by Eq. (13), taking into consideration a magnitude of 6.4.

GMDD
8, 4487–4544, 2015

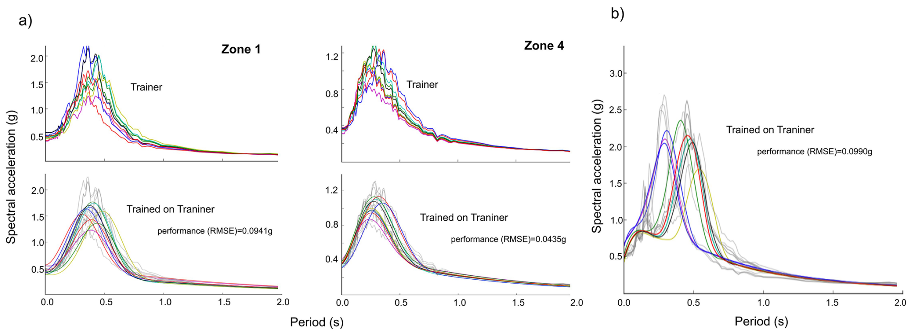

Figure 7. Performance of SPECTRA: **(a)** stratigraphic seismic response with a damping of 0.05 regarding some trainer V_S, h profiles of the SRS (all graphics are reported in the Supplement). The resulting performance defined by RMSE (g) are: zone 1 = 0.0941; zone 2 = 0.0862; zone 3 = 0.0544; zone 4 = 0.0435; zone 5 = 0.0370; zone 6 (non rigid rock in outcropping) = 0.0032; zone 7 (rigid rock in outcropping) = 0.0045; zone 8 = 0.0394 **(b)** example on stratigraphic seismic responses that show a large spectral variability; the trainer spectra are obtained by the notable increasing of the top-layer thicknesses in the zone 1 models.

GMDD
8, 4487–4544, 2015

A simulator for mapped seismic response using a hybrid model

G. Grelle et al.

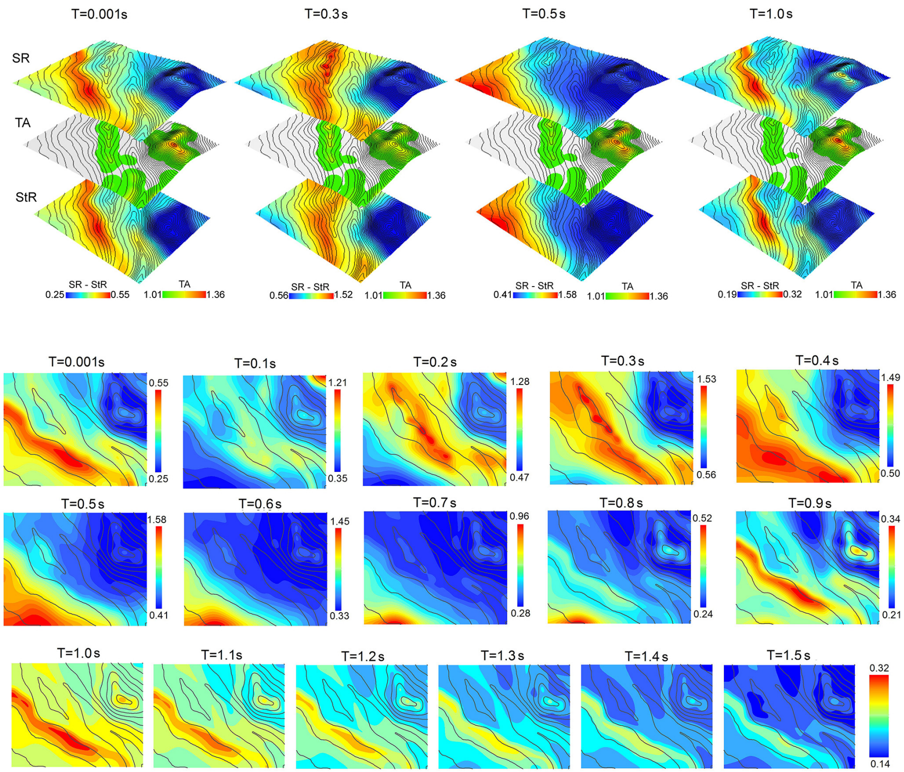

Figure 8. Set of seismic response maps for different periods. The combined effect of the stratigraphic and topographic features are shown at the top of the figure; StR is the stratigraphic seismic response, TA is the topographic amplification and SR is the seismic response.

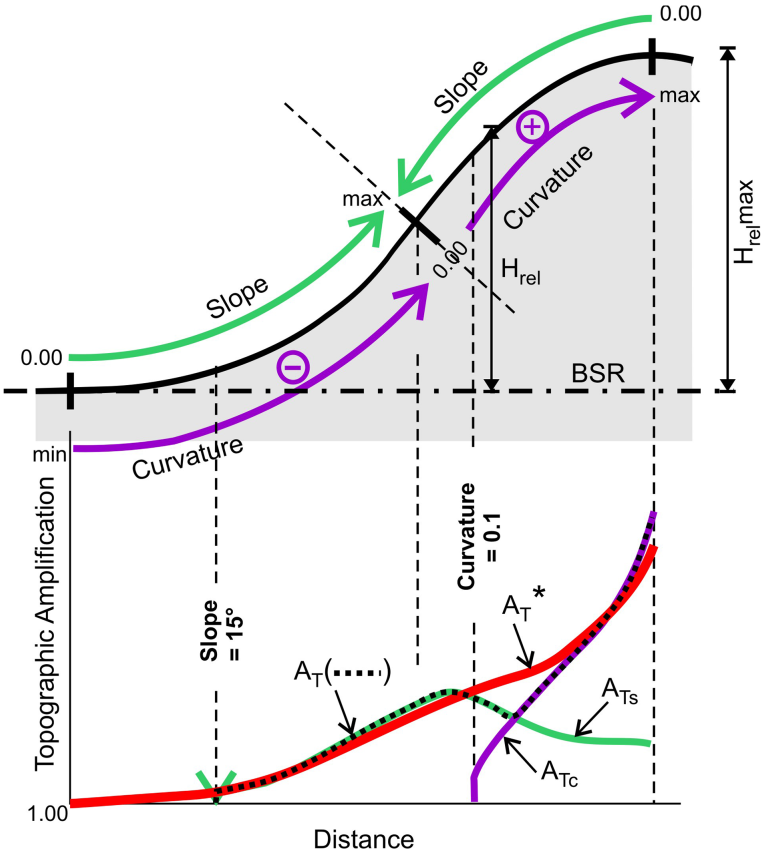

Figure 9. The behaviour components of the topographic amplification model in relation to the distribution of the GIS-topographic attributes (DEM, slope and curvature) along an isolated half-relief.

GMDD
8, 4487–4544, 2015

A simulator for mapped seismic response using a hybrid model

G. Grelle et al.

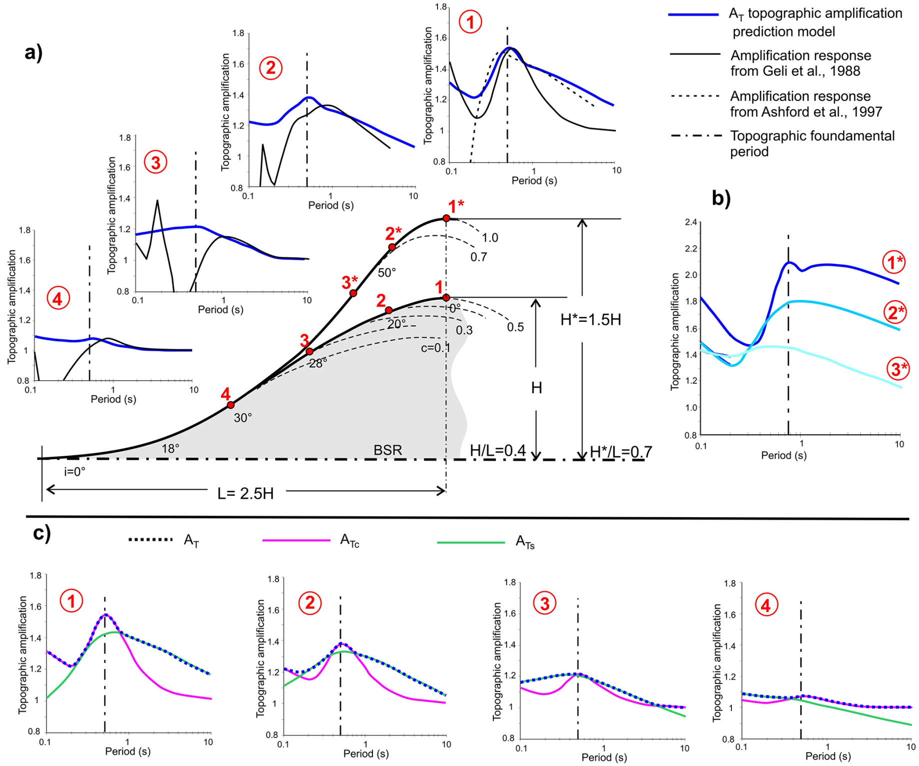

Figure 10. Performance of the topographic prediction model, A_T, along an isolate half-relief; this is similar to that used in the numerical simulation by Geli et al. (1988). **(a)** The simulation considers vertical incident SH waves; in the same way, the Ashford et al. (1997) simulation analysis regards the ridge of the relief with a slope angle of 90°; **(b)** topographic prediction projected on a more pronounced relief; **(c)** topographic prediction model A_T illustrated in term of combined shape of A_{Tc} and A_{Ts} models.

GMDD
8, 4487–4544, 2015

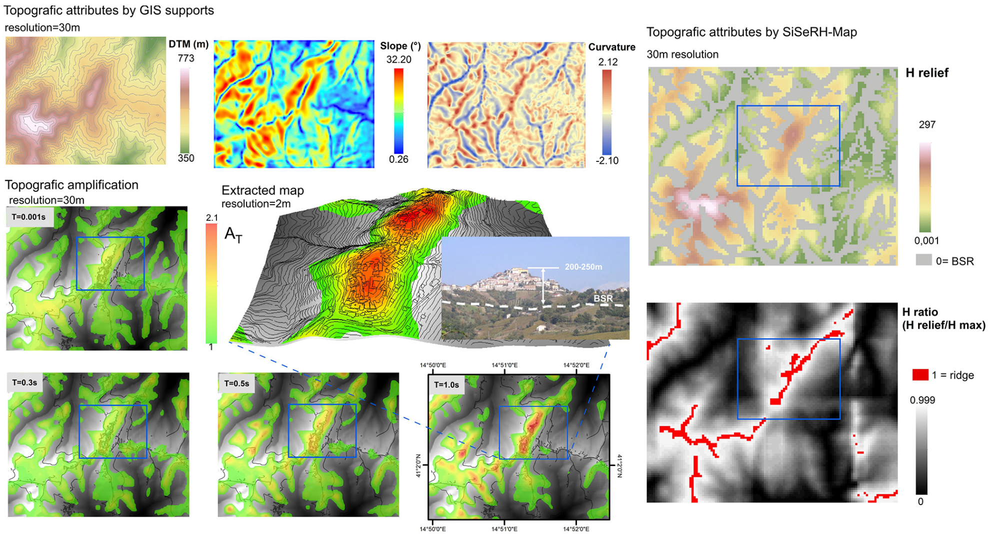

Figure 11. Topographic amplification computed on a real hill-mountain area of southern Italy: blue box is the automatic splitting map of the urbanized area of the village of Montefusco.

GMDD
8, 4487–4544, 2015

A simulator for mapped seismic response using a hybrid model

G. Grelle et al.

Title Page
Abstract | Introduction
Conclusions | References
Tables | Figures
◀| |▶
◀ ▶
Back | Close
Full Screen / Esc
Printer-friendly Version
Interactive Discussion

GMDD
8, 4487–4544, 2015

Title Page
Abstract | Introduction
Conclusions | References
Tables | Figures
◀| |▶
◀ ▶
Back | Close
Full Screen / Esc
Printer-friendly Version
Interactive Discussion

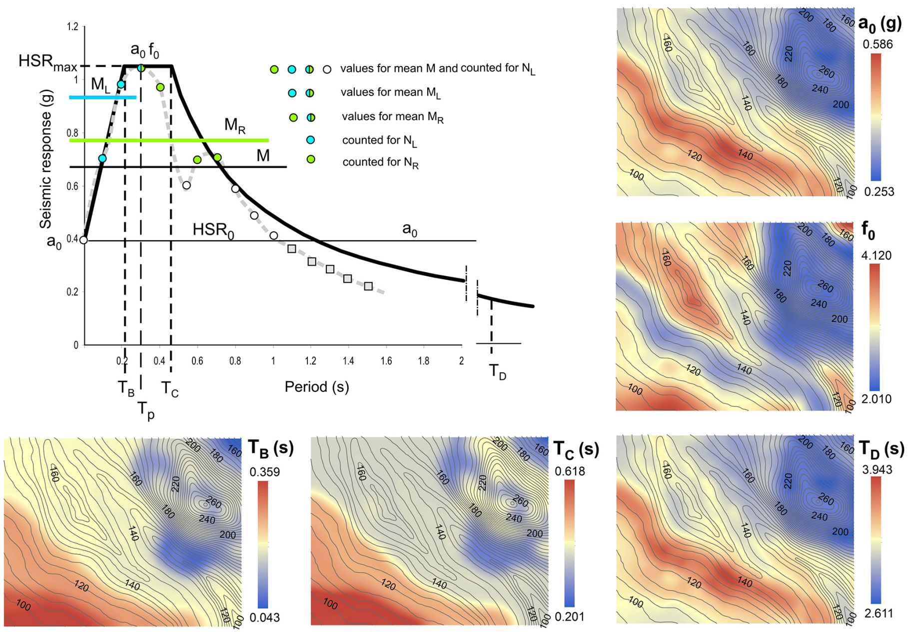

Figure 12. Enveloping model that creates the design spectrum; around it, the mapping distribution of the characteristic parameters of the design spectra, are shown.

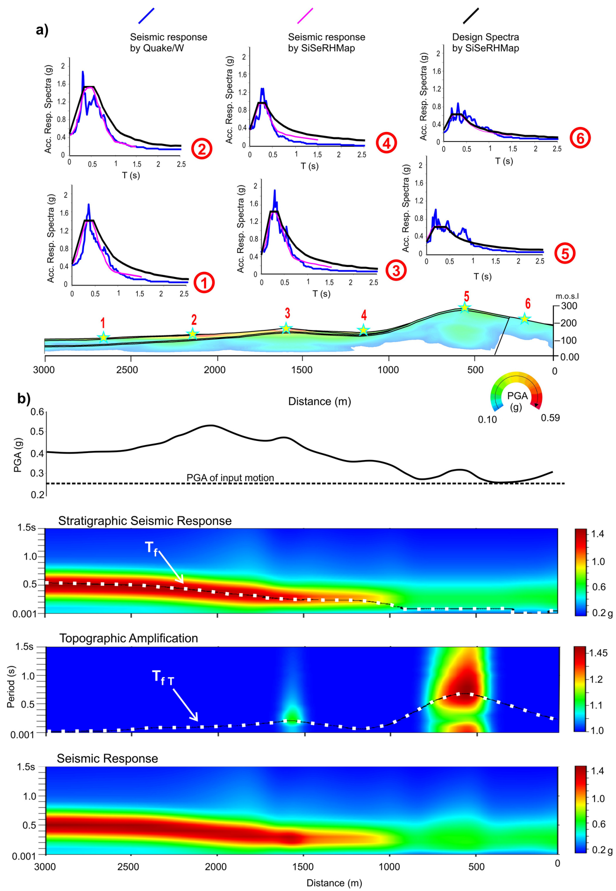

Figure 13. Comparison between the seismic response by SiSeRHMap and the Quake/W finite element method on an across-section showed in Fig. 1.

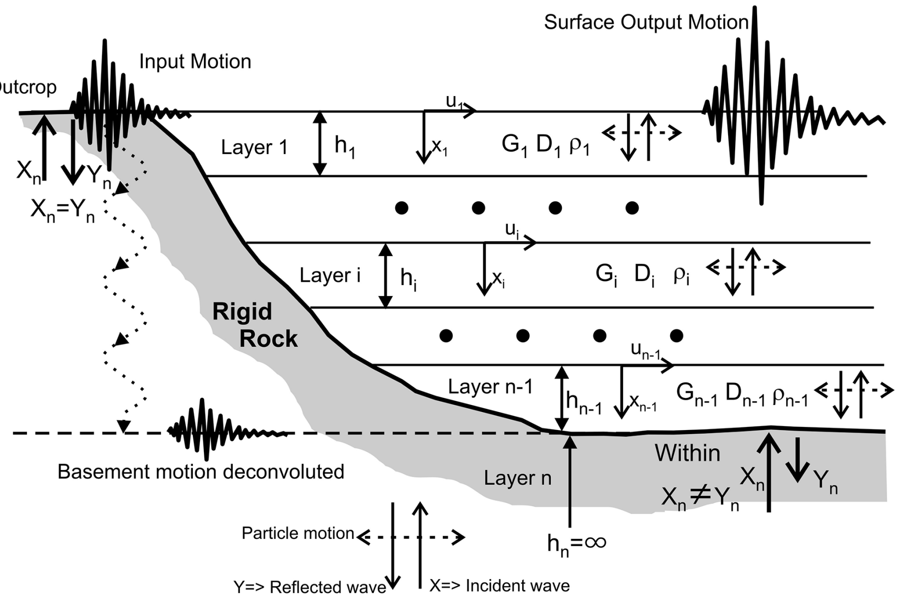

Figure A1. Stratigraphic amplification model (mod.3) consisting of a one-dimensional layered system composed of nonlinear viscoelastic soils covering the rigid viscoelastic bedrock.

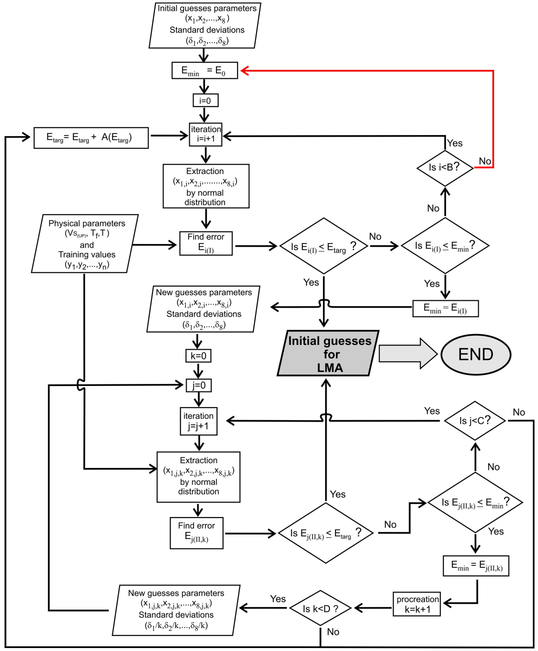

Figure B1. The Evolutionary Algorithm (EA) scheme: x and δ are the mean and the standard deviation in normal distribution; **I** and **II** indicate the first and the second phase; i, j are the generic populations; k is the ranking of the generation in the second phase; E_0 is the initial error (100); E_{min} is the current error; E_{targ} is the initial error target, it depends on the number of lithodynamic units in the V_S,h trainer model and the number of trainer models (0.005 to 0.05); A is the increased ratio of the E_{targ} (0.02); B is the number of the generated population (2000) before the mass extinction (red flow line); C is the max number of populations permitted in a generation of the second level (100); D is the number of the generation in the second phase (4).

GMDD
8, 4487–4544, 2015
A simulator for mapped seismic response using a hybrid model
G. Grelle et al.